Athens Journal of Technology & Engineering

Quarterly Academic Periodical, Volume 9, Issue 1, March 2022
URL: https://www.athensjournals.gr/ajte
Email: journals@atiner.gr
e-ISSN: 2241-8237 DOI: 10.30958/ajte

Front Pages

Athens Journal of Technology & Engineering

Published by the Athens Institute for Education and Research (ATINER)

****

*

ATINER is an Athens-based World Association of Academics and Researchers based in Athens. ATINER is an independent and non-profit Association with a Mission to become a forum where Academics and Researchers from all over the world can meet in Athens, exchange ideas on their research and discuss future developments in their disciplines, as well as engage with professionals from other fields. Athens was chosen because of its long history of academic gatherings, which go back thousands of years to Plato's Academy and Aristotle's Lyceum. Both these historic places are within walking distance from ATINER's downtown offices. Since antiquity, Athens was an open city. In the words of Pericles, Athens"…is open to the world, we never expel a foreigner from learning or seeing". ("Pericles' Funeral Oration", in Thucydides, The History of the Peloponnesian War). It is ATINER's mission to revive the glory of Ancient Athens by inviting the World Academic Community to the city, to learn from each other in an environment of freedom and respect for other people's opinions and beliefs. After all, the free expression of one's opinion formed the basis for the development of democracy, and Athens was its cradle. As it turned out, the Golden Age of Athens was in fact, the Golden Age of the Western Civilization. Education and (Re)searching for the 'truth' are the pillars of any free (democratic) society. This is the reason why Education and Research are the two core words in ATINER's name.

****

The ***Athens Journal of Technology & Engineering (AJTE)*** is an Open Access quarterly double-blind peer reviewed journal and considers papers from all areas engineering (civil, electrical, mechanical, industrial, computer, transportation etc), technology, innovation, new methods of production and management, and industrial organization. Many of the papers published in this journal have been presented at the various conferences sponsored by the Engineering & Architecture Division of the Athens Institute for Education and Research (ATINER). All papers are subject to ATINER's Publication Ethical Policy and Statement.

The Athens Journal of Technology & Engineering
ISSN NUMBER: 2241-8237- DOI: 10.30958/ajte
Volume 9, Issue 1, March 2022
Download the entire issue (PDF)

Athens Journal of Technology & Engineering
Editorial and Reviewers' Board

President's Message

All ATINER's publications including its e-journals are open access without any costs (submission, processing, publishing, open access paid by authors, open access paid by readers etc.) and is independent of presentations at any of the many small events (conferences, symposiums, forums, colloquiums, courses, roundtable discussions) organized by ATINER throughout the year and entail significant costs of participating. The intellectual property rights of the submitting papers remain with the author. Before you submit, please make sure your paper meets the basic academic standards, which includes proper English. Some articles will be selected from the numerous papers that have been presented at the various annual international academic conferences organized by the different divisions and units of the Athens Institute for Education and Research. The plethora of papers presented every year will enable the editorial board of each journal to select the best, and in so doing produce a top-quality academic journal. In addition to papers presented, ATINER will encourage the independent submission of papers to be evaluated for publication.

The current issue is the first of the ninth volume of the *Athens Journal of Technology & Engineering (AJTE)*, published by the Engineering & Architecture Division of ATINER.

Gregory T. Papanikos, President, ATINER.

Athens Institute for Education and Research

A World Association of Academics and Researchers

12th Annual International Conference on Civil Engineering
20-23 June 2022, Athens, Greece

The Civil Engineering Unit of ATINER is organizing its **12th Annual International Conference on Civil Engineering, 20-23 June 2022, Athens, Greece** sponsored by the Athens Journal of Technology & Engineering. The aim of the conference is to bring together academics and researchers of all areas of Civil Engineering other related areas. You may participate as stream leader, presenter of one paper, chair of a session or observer. Please submit a proposal using the form available (https://www.atiner.gr/2022/FORM-CIV.doc).

Academic Members Responsible for the Conference

- **Dr. Dimitrios Goulias**, Head, Civil Engineering Unit, ATINER and Associate Professor & Director of Undergraduate Studies Civil & Environmental Engineering Department, University of Maryland, USA.

Important Dates

- Abstract Submission: **28 February 2022**
- Acceptance of Abstract: 4 Weeks after Submission
- Submission of Paper: **23 May 2022**

Social and Educational Program

The Social Program Emphasizes the Educational Aspect of the Academic Meetings of Atiner.

- Greek Night Entertainment (This is the official dinner of the conference)
- Athens Sightseeing: Old and New-An Educational Urban Walk
- Social Dinner
- Mycenae Visit
- Exploration of the Aegean Islands
- Delphi Visit
- Ancient Corinth and Cape Sounion

Conference Fees

Conference fees vary from 400€ to 2000€
Details can be found at: https://www.atiner.gr/fees

10th Annual International Conference on Industrial, Systems and Design Engineering, 20-23 June 2022, Athens, Greece

The Industrial Engineering Unit of ATINER will hold its **10th Annual International Conference on Industrial, Systems and Design Engineering, 20-23 June 2022, Athens, Greece** sponsored by the Athens Journal of Technology & Engineering.The aim of the conference is to bring together academics, researchers and professionals in areas of Industrial, Systems, Design Engineering and related subjects. You may participate as stream leader, presenter of one paper, chair of a session or observer. Please submit a proposal using the form available (https://www.atiner.gr/2022/FORM-IND.doc).

Important Dates

- Abstract Submission: **28 February 2022**
- Acceptance of Abstract: 4 Weeks after Submission
- Submission of Paper: **23 May 2022**

Academic Member Responsible for the Conference

- **Dr. Theodore Trafalis**, Director, Engineering & Architecture Division, ATINER, Professor of Industrial & Systems Engineering and Director, Optimization & Intelligent Systems Laboratory, The University of Oklahoma, USA.

Social and Educational Program

The Social Program Emphasizes the Educational Aspect of the Academic Meetings of Atiner.

- Greek Night Entertainment (This is the official dinner of the conference)
- Athens Sightseeing: Old and New-An Educational Urban Walk
- Social Dinner
- Mycenae Visit
- Exploration of the Aegean Islands
- Delphi Visit
- Ancient Corinth and Cape Sounion

More information can be found here: https://www.atiner.gr/social-program

Conference Fees

Conference fees vary from 400€ to 2000€
Details can be found at: https://www.atiner.gr/fees

Athens Journal of Technology and Engineering - Volume 9, Issue 1, March 2022 – Pages 9-24

Flexible Robot Programming using Solid Edge's "Alternative Assemblies"

By Norman Urs Baier[*] & Joel Costan Zovi[±]

Many assembly processes in small and medium-sized enterprises are still performed by human labour. One reason for this is the need for another expert to program the robot, which would simply not fit into the company structure. To address this issue a solution is developed, which allows to program the robot directly out of the CAD software. The positions of the parts are read out of the CAD file. Specific assembly instructions have to be given by the assembly developer and integrated in the tree structure of the CAD. To avoid collisions and ensure correct insertion angles, additional waypoints are given by alternate assemblies, a functionality within Solid Edge to create and use variations of an assembly.

Keywords: *assembly, task planning, intelligent and flexible manufacturing, CAD*

Introduction

The classical use of an industrial robot is within a repetitive process. It is taught a few positions with the teach panel or by other means and then it starts doing its task. If the process is a manufacturing or assembly process, then most often a single robot performs tiny subtasks of the whole process and most often the production volume is high. Markis et al. (2016) distinguish four different production paradigms, namely fixed automation, robotic automation, human-robot collaboration, and manual assembly. As production costs do not scale with lot size for manual assembly this is the solution for smallest lot sizes, whereas fixed automation is for rather large lot sizes. For lot sizes in between, though, robots may also be deployed profiatinerly. Depending on lot size and complexity of the manufacturing process different strategies have been developed.

For some manufacturing processes of more complex nature, the robot will need to cowork with a human operator even in the foreseeable future. This situation requires different programming paradigms than situations in which the robot alone is capable of completing the tasks, but some single elements change after very small batch sizes. Wang et al. (2019a) have identified and named four different forms of human-robot relationships: coexistence, cooperation, interaction, and collaboration. Clearly, in case of collaboration the robot needs to understand the human and hence appropriate programming paradigms need to be available. These need to include on one hand the ability to learn quickly from human interaction

[*]Professor for Control Engineering and Mechatronics, Bern University of Applied Sciences, Switzerland.
[±]Microcut Ltd, Switzerland.

despite possible ambiguity (Thomaz and Breazeal 2008, Wang et al. 2019b) and on the other hand they need to establish possible ways the human can express himself toward the robot (Tsarouchi et al. 2016, Cserteg et al. 2018).

In contrast, many manufacturing processes performed in small and medium sized enterprises (SME) could be performed by a robot without the help of a human co-worker. There are several reasons why often manual labour is preferred in SMEs. One of them is that classical robots take up too much space, because they need to be behind fences (Perzylo et al. 2016), a problem solved to a large extent with collaborative robots in a coexistence scenario. Another reason is the programming effort and the apprehension an expert might be needed to perform the programming (Perzylo et al. 2016). The usability of the user interfaces of collaborative robots has been analysed by Schmidbauer et al. (2020). To address the need for effortless deploying of robots, software has been proposed by fortiss, for example: Perzylo et al. (2019) describe a software which allows to program a robot by manipulating physical parts and drawings of them on screen. The assembly itself can be divided in subtasks, each of which is capable of performing a particular action. These are called skill primitives and depending on robot and sensors installed, different skill primitives can be realised (Watson et al. 2020).

Alternatively, manufacturing or assembly data can be extracted directly out of existent CAD files; an approach which has been identified as promising by von Drigalski et al. (2020). Known in literature is a strategy called "assembly by disassembly", it proved to work for the assembly of different types of housings (Michniewicz et al. 2016). Recently, strategies have been published in which the tree structure in the CAD file is used to harbour instructions for assembly (Linnerud et al. 2019, Transeth et al. 2020).

A link still not duly carved out to or opinion is how existing work processes in SMEs may be altered such that in the end a robot can assemble the designed item. Particularly, it may not be necessary or not even desired that the assembly sequence is generated automatically. Instead, usually the product designer has a clear idea already how the item shall be assembled, and the robot should do, the way the designer intended it to go on. Hence, it should blend in with existing development and design processes, which most often are amended CAD files. Furthermore, to increase the acceptance of robots in SMEs the robot itself should blend in with existing workplaces traditionally designed for humans. It should be able to use those tools, which humans use as well. In this paper we present a set-up to perform assembly with a robot, which addresses the problems within the above-mentioned frame.

Bin picking, on the other hand, is not considered as within the frame: all objects and items are provided at known locations. Provisioning is an important part in a complete assembly process; however, it can be solved detached from the actual assembly process.

Methodology

An example item is assembled with an off-the-shelf collaborative robot. In this section we give all the details of the example item, the robot, the tools, and

software, which were used for the task.

Example Item: Spur Gear Unit

To develop and assess the automatic programming, an example item was selected. The requirements for the example item were:

- size such that an ordinary collaborative robot can handle it,
- composed of a manageable number of parts,
- different assembly tasks involved during assembly,
- preferably an item, which is publicly available for purchase.

Figure 1. *Exploded Drawing of the Spur Gear Unit*

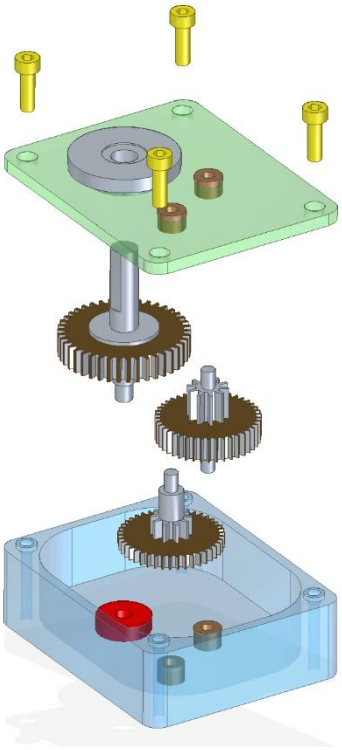

Figure 2. *Spur Gear Unit before Assembly, Arranged on the Mounting Plate*

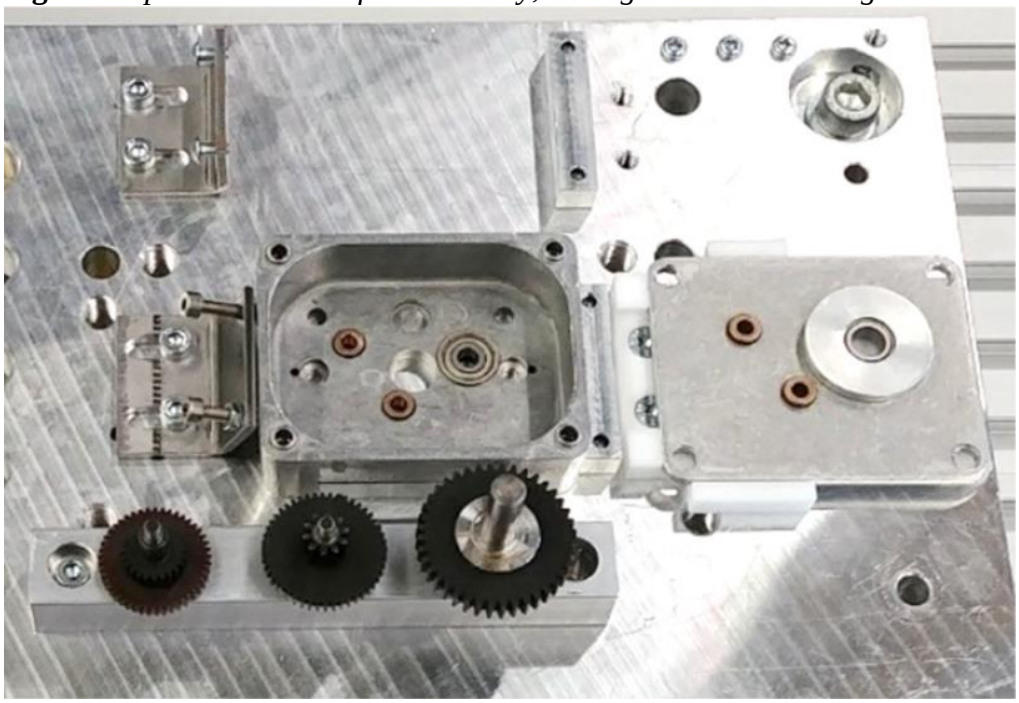

The choice fell on a spur gear unit of Hilba, more precisely the model GOBUN5713FR100-01. It consists of a housing with bearings, 3 gearwheels on axes fitted to the bearings and a lid screwed on the housing. Its assembly consists of inserting the gearwheels into the bearings. For the second and third gearwheel the correct interleaving has to be observed. Furthermore, posing of the lid is an involved process. It includes three steps and screwing. The lid comprises the bearings for the axes of the gearwheels. First, it has to be posed and then the correct insertion of all three axes has to be verified. For the screwing of the lid, a tool (screwdriver) needs to be used. Figures 1 and 2 show the spur gear unit in a disassembled state and as an exploded drawing.

Robotic Arm, Gripper, Sensors and Tools

There are no particular requirements for the robot, on the contrary, the less particular the robot is, the better the results can be ported to other installations. For reasons of availability, the choice fell on a F&P Robotics P-Rob 2. This is a 6 DOF industrial robot with a straight idle position. It is originally equipped with a servo gripper, but for this work a custom hand with three separate pneumatic grippers is installed.

Furthermore, the HEX-E force torque sensor of On Robot A/S is installed on the robotic arm and an electric screwdriver is mounted within the reach of the robotic arm. The screwdriver can be switched on and off through the digital connections of the robotic arm and hence controlled through the proprietary robot software myP (F&P Robotics 2018a, Mišeikis et al. 2020).

Communication with and triggering of routines within the robotic arm was done through a TCP-socket. Through the socket myP provides possibilities to

trigger functions and procedures written in Python. With the help of those the adoption of poses can be triggered, and the digital IO-connections can be read or set. myP offers an extensive set of functions to do so (F&P Robotics 2018b). The functions that are used in the proposed realisation are:

- `write_digital_outputs()`: to control attached electrical equipment like the screwdriver or the pneumatic valves to close the grippers,
- `read_digital_inputs()`: to observe the feedback on torque and general errors of the screwdriver,
- `run_advanced_path()`: to make the robotic arm move like required by the assembly program,
- `read_tcp_pose()`: to read out the current position of the tool center point and correspondingly continue with the assembly.

Other functions like `close_gripper()` and `open_gripper()` are also implemented in myP, but have not been used. These two functions in particular because other grippers have been installed. No myP-functions are used to read out the HEX-E force torque sensor, it is connected directly to the PC running the assembly program.

CAD Software

In order to blend in as good as possible with existing workflows, the interface to the CAD-data is set up on application layer, not on file layer. This means Step-files or similar files are not considered as input source, but an appropriate and existing API towards a widespread CAD software suite is used. Here Solid Edge was used for the implementation; among the more important softwares according to market share (Warfield 2020), it proved to be most easy to interface to: Through the libraries *Interop.SolidEdge* and *SolidEdge.Community* data contained in a Solid Edge design can be extracted and manipulated in a straightforward manner from any C# software project.

Product Development and Assembly Development

For our method we started from the working assumption that product development and assembly development are two separate steps in the workflow of the manufacturer. The method does not aim at eliminating assembly development by the help of artificial intelligence or other means. So, for the assembly itself it is assumed that the assembly developer performing the actual development will receive all data concerning the product to be assembled in form of a CAD file and that the technician then starts to plan in which order the individual components need to be aligned and merged and what particular steps are involved.

In fact, assembly development is always involved in conjunction with product development, however it can take a different appearance depending on the company carrying out the product development. The method presented here requires the assembly development to be carried out in the CAD software as

opposed to more manual workflows involving text documents and photos of an example assembly, which is still very common in smaller companies.

Performing the assembly development in CAD is advantageous for a work process where assembly development is performed by a constructing engineer and most advantageous if it is performed right after product development by the same engineer, who has performed the product development. The engineer can then exploit all the skills already used during design phase. Such a process would ideally fit very small companies.

Results

In the current implementation a software procedure written in C# (the program) connects to the CAD data on one side and the robotic arm on the other side. Before focusing on how information is processed and transmitted from one element of the installation to the other, it is important to specify some of the details of Solid Edge, which are important for the implementation.

Alternate Assemblies for Additional Waypoints or Movements

In common industrial workflows the assembly developer has the crucial task to assure that gripping the part to be added to the assembly is possible and the joining position can be reached with the defined grip, independent of the fact if the assembly is performed by humans or robots. To verify if the grip is possible, the gripper is represented in the CAD tool. To define the actual joining movement, additional waypoints may be necessary. Here, alternate assemblies are used to define these waypoints. "Alternate assemblies" is the name of a functionality within Solid Edge, which can be used to manage variations of an assembly (Siemens Product Lifecycle Management Software Inc. 2011). It allows to store an assembly in different configurations, showing the parts, out of which it is assembled, in different locations and orientations. It can also be used to store configurations, in which some parts differ. Without this functionality, it would be less convenient to mark parts as identical and keep the different variants of the assembly in place. With this functionality, the presence and location of the assembled parts can be stored in a single file for different configurations. Within Solid Edge, the different assembly configurations are called members.

Figure 3. *Member2 Showing Two Different Intermediate Positions of the First Gearwheel*

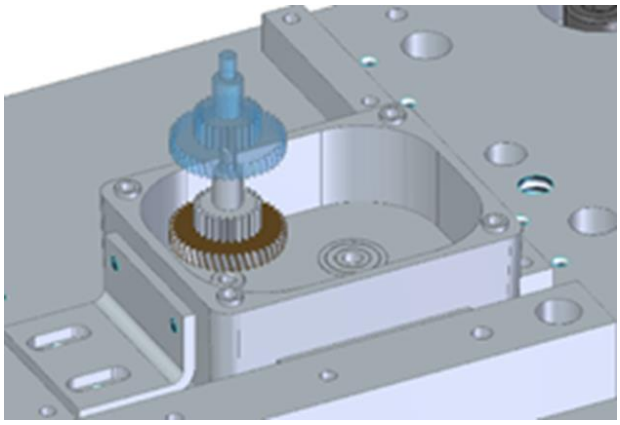

In our implementation the members are used to define subsequent poses of the element to be joined. Hence, in one member the assembly is shown with the part currently to be joined in its final location, while it is shown in other members in intermediate positions. Figure 3 shows two different alternate assemblies in an overlay: In one alternate assembly (shown in transparent blueish) the first gearwheel has an intermediate position, in another (shown solid) it has its final position. With these means, the assembly developer can harness the robot very precisely. Furthermore, through commands written into the placement name (described below) the program can be informed that a particular skill is necessary to complete the assembly step. Instancing the step shown in Figure 3, most often mounting an axis into its bearing cannot be done with a simple linear movement but requires a sequence of movements and measurements. One way to give the robot the ability to exhibit more elaborate behavior than simple linear movements is skills (Thomas et al. 2003). The skills, which are necessary to assemble the spur gear unit, and hence are now already implemented in the program are also described below.

Individual parts in the CAD file can have a different origin. It is common practice to use third party parts in assemblies and import the corresponding part from a CAD library of the supplier of the part and the library. Therefore, the origin of the coordinate system of a part cannot reliably be used to determine the gripping pose, because the supplier can put it anywhere. As a solution the gripper is introduced into the CAD drawing. The task of the assembly developer becomes then to align the gripper with the part to be handled, which can be done with few clicks by a trained designer. Display the gripper in the assembly is recommended anyway, as it also allows to check for collision free gripping and releasing while planning the assembly procedure. The assembly showing the part to be handled together with the gripper is shown in Figure 4.

In our implementation the numbering scheme of the members and the parts within the members are used to specify the assembly order.

Figure 4. *Member1 Showing Gripper Mounting Plate and Final Joining Position of the First Gearwheel*

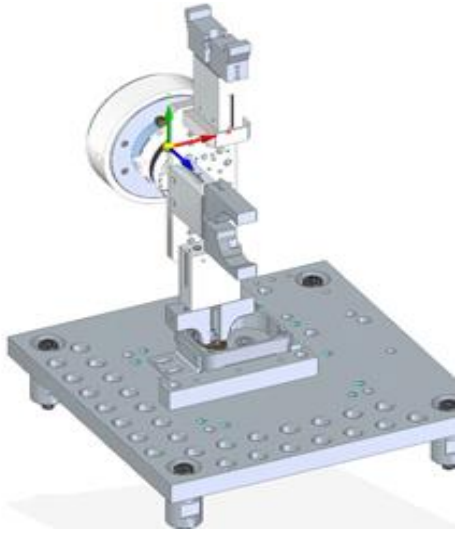

Interfaces & Structure

Figure 5 shows all involved elements of the installation used in the current implementation. The central element is the above-mentioned C# program, which connects

- to Solid Edge with the help of the corresponding libraries,
- to the software "myP" on the robotic arm through TCP sockets, and
- to the force torque sensor through its USB interface.

The robotic arm connects

- to the electrical screwdriver with its control box, and
- to the valve controlling the three pneumatic grippers,

both through its digital IO ports.

Figure 5. *Interfaces and Structure of the Hardware and Software Components*

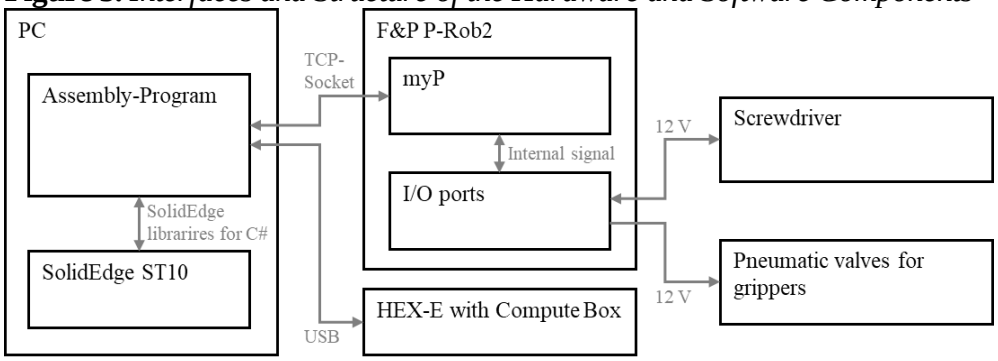

The interface of the program to the robotic arm and accessories is straightforward: Through this channel merely pose and gripping instructions are transmitted in an implicit way by triggering the functions described in the previous section. The data processing, which breaks down the complex assembly task to single poses to reach and gripping instructions, takes place beforehand when the program reads out the instructions of the assembly developer stored in the CAD file.

Instructions in the CAD File

During assembly development, necessary information to successfully perform the assembly is created. This information is stored in the CAD file. This includes information on possible tools that are used during the joining, where individual parts are located and the pose with which the gripper has to reach for those parts.

Solid Edge provides a "placement name" to describe a particular entity of the component used. It can be user defined and here, it is used to store information on the assembly process. The existing placement name is augmented with key-value pairs describing the action that needs to be performed. All implemented keys are shown in Table 1. The key-value pairs are separated by a semicolon. How this looks in Solid Edge is shown by the screenshot in Figure 6.

Figure 6. *Screenshot Showing the Highlighted Member in the Edgebar and the Pathfinder with Parts Having a Custom Placement Name*

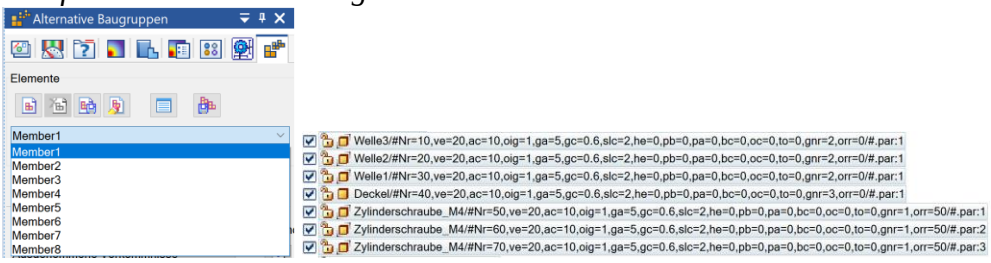

Table 1. *Possible Qualifiers in Placement Name*

Key	Meaning
`nr`	Sequential number of the assembly step
`ve`	Velocity
`ac`	Acceleration
`oig`	1: Gripping outward, 2: Gripping inward
`he`	Tool use, 1: Screwdriver
`pb`	Intermediate position
`oc`	Gripper open or closed, 1: Open, 2: Closed
`to`	Skill primitive, 1: bolt into bearing, 4: gearwheel
`gnr`	Gripper number
`orr`	Retraction

The order in which parts have to be gripped and joined is specified by the value given with the key `nr`. Furthermore, `ve` and `ac` keys can be given to limit velocities and accelerations during that step. Whether or not the part has to be

gripped outward or inward is specified by key `oig`.

In case the part is not gripped or handled directly by the gripper, the key `he` is used to specify which tool has to be used. Currently only the screwdriver is implemented. With the key `pb` intermediate positions can be specified: The part will be moved successively from the position with the highest `pb` number to the position with the lowest `pb` number. Hence, a trajectory with angles can be forced. This may be necessary to fit the gearwheels or the lid onto the assembly, or whenever elements of the assembly have to be avoided during joining. The key `oc` allows to close or open the gripper at particular position.

To specify how the joining has to be performed, the key `to` is used. With this key, the program is told what substeps are involved during the joining. Currently two different situations are implemented: A bolt has to be fit into a bearing (value 1) and a gearwheel has to be interlocked (value 4). The solutions involve skill primitives and are detailed in the next section.

Which gripper shall be used to grip the part can be specified with the help of the key `gnr`. The key `orr` is most useful in conjunction with the key `pb`. With its help a retraction distance can be specified. The gripper is then retraced for the specified distance along the final axis and does not rewind the path specified by the intermediate positions given by `pb`.

Skill Primitives

The skill primitives and the associated transitions are usually organised in nets like the one shown in

Figure **7** (Thomas et al. 2003). In the context of the assembly considered here, skill primitive nets were created for mounting axes, interlocking gear wheels and mounting the cover lid. In these tasks the skill primitive nets are a way to handle the uncertainty, which could prevent the task from finishing successfully otherwise. They are triggered through particular commands described above. When the assembly developer declares for example that the current part is an axle, which should go into a bearing, then the program calls the associated skill primitive net implemented in the C# code.

Figure 7. *Skill Primitive Net for Mounting an Axle*

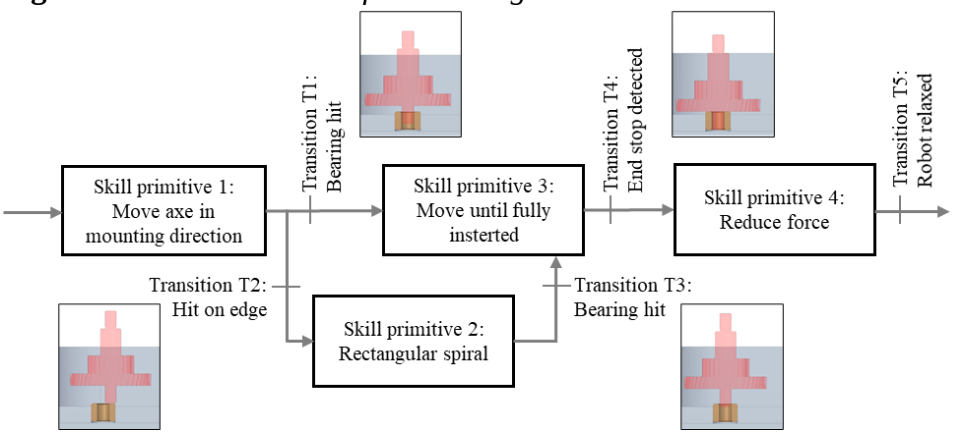

The skill primitive net for mounting an axle is composed of four skill primitives. A block diagram for it is shown in Figure 7.

Skill primitive 1 involves moving the axle along the mounting direction. Either until a critical depth is reached, or the force measurement increases. More precisely, if the measured position exceeds the position, which can be reached when the axle hits the edge, the transition T1 is taken and skill primitive 3 "move the axle vertically until fully inserted" is activated. Otherwise, transition T2 is taken and skill primitive 2 "moving the axle in the shape of a rectangular spiral" is activated first, before skill primitive 3 is activated via transition T3. This happens when the vertical force decreases significantly. The last skill primitive in this net is "reduce inserting force" and the transition between skill primitives 3 and 4 occurs when force measurements increase while position measurements stall. The skill primitive net is left when the force measurement confirms the relaxed pose.

Figure 8. *Skill Primitive Net for Aligning Gear Wheels*

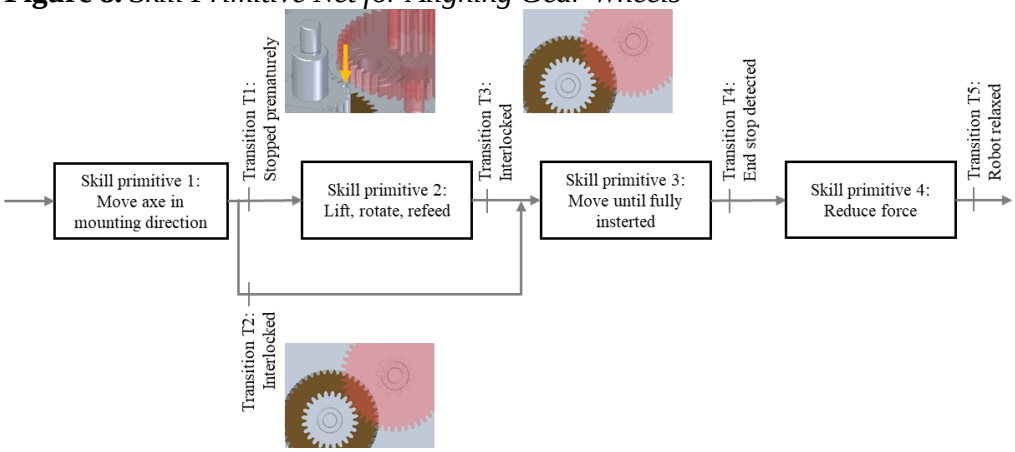

When gear wheels are successively assembled in a spur gear unit, the subsequently added gear wheels have to be aligned to the previously mounted gear wheel. For this situation we created another skill primitive net, which is shown in Figure 8. The outline is quite similar to the first skill primitive net for mounting an axle. In our application the skill primitive net for mounting an axle is always executed before the skill primitive net described here. The defined skill primitives are:

1. move gear wheel in axle direction,
2. lift, rotate and press gear wheel in axle direction again,
3. move in axle direction until final position is reached,
4. reduce inserting force.

The possible transitions are from skill primitive 1 to skill primitive 2 when force measurements increase while not having reached the required vertical position or to skill primitive 3 in case the gear wheels were already aligned and the vertical position was reached without a significant increase in vertical force the same criterion forms the transition from skill primitive 2 to skill primitive 3 and

the transition from skill primitive 3 to 4 occurs when the force increases while the position measurement is reached the final state. The skill primitive net is left from skill primitive 4, when the force measurement has reached a relaxed state.

Calibration of the Mounting Plate

In our example, the assembly takes place on a mounting plate. It serves as a reference for all parts that take place in the assembly. The different joining operations during the assembly require the positions of the joined part to be known with an appropriate precision. The worse the precision is, the longer the joining can take, as the robotic arm has to search for the correct mechanical stops.

The assembly performance benefits when the physical pose of the mounting plate coincides precisely with the pose of its digital representation, such that tolerances in mounting plate and robot links are compensated for either by mechanical manipulation or by calculations. For the purpose of calibration, the mounting plate has a number of holes in it that can be used in the process of calibration. The precise process of calibration we adopted for consists of both a mechanical adjustment and a computational correction.

First the orientation of the mounting plate around its vertical axis is set mechanically. The robot gripper is lowered so that the mounting plate can be oriented flush with the yaw angle of the gripper. Next, rods are used to align the gripper with the mounting plate for pitch and roll angles of the gripper (Figure 9). In the end correction angles for pitch and roll for each gripper are known. These depend heavily on the individual robot and the force-torque-sensor.

Figure 9. *Procedure to Calibrate Mounting Plate: First the Yaw Angle around the Blue Arrow is Adjusted Mechanically (Left, Hatched Surface), then the Pitch Angle Around the Red Arrow (Middle) and the Roll Angle around the Green Arrow (Right) Are Measured with the Help of a Bolt*

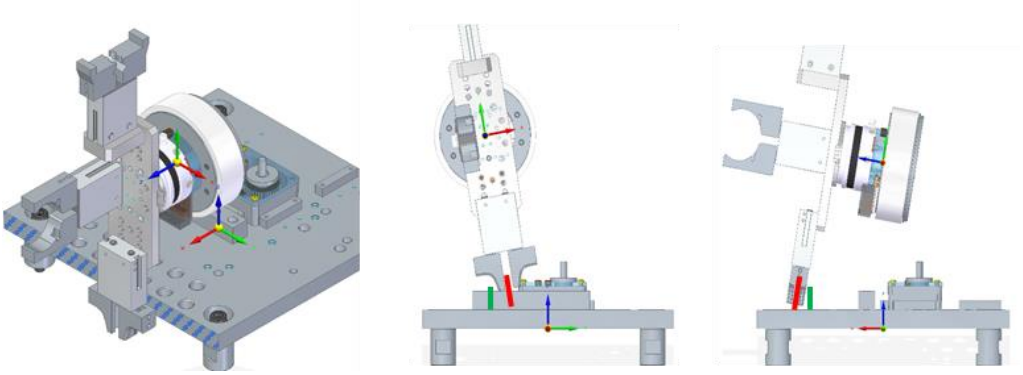

With the previous steps the orientation of the mounting plate with respect to the CAD data has been assessed, however, discrepancies in the position data are still possible. To close that gap the robot is again made holding a rod, which this time is inserted into three of the holes in the mounting plate. When inserted in the hole, the robot pose is tuned such that the force measures zero and the corresponding positions from the robot control are read out and hence the position vectors of the

three centres of the holes are known. By simple vector subtraction and normalisation, the coordinate system of the mounting plate can be calculated. Now, given a pose of a part in the CAD system, the corresponding pose of the part on the mounting plate easily calculated.

Sequences of the Program in Chronological Order

To read out the position information and to prepare them for use in the assembly command for the robot, the alternate assemblies are run through in order. The libraries Interop.SolidEdge and SolidEdge.Community are used to access Solid Edge through the API and load the alternate assemblies to read out the position of the part whose turn it is.

The alternate assemblies are named Member and numbered through in our implementation: "`Member1`, `Member2`, …". In the first member (`Member1`) the assembly is drawn in its final assembled state. The assembly program begins by reading out `Member1`. One fundamental position information which is currently stored in `Member1` is the position of the gripper itself: The position of the gripper, when the robot is in its rest position is drawn in `Member1`.

The order of the assembly is given in the placement name by the attribute "`nr`" visible in Figure 6. In steps of 10 this attribute directly gives the order of the assembly, whereas the final assembled position is given in the alternate assembly with the name "`Member1`". If there is another alternate assembly showing the same part in another pose, then the robot has first to reach this pose before it brings the part to the final pose.

In the end of that step all data has been extracted from Solid Edge and has been stored in an array. The data in the array are insertion and final positions and the command string, the assembly engineer had put in the placement name.

To make the data accessible and store them for future use, they are stored in a file in JSON-format.

Next, the position data together with the instructions in the placement name need to be processed, with the aim to generate a sequence of commands the robot understands. The sequence will then be sent to the robot to perform the assembly.

The table previously stored in JSON-format is already ordered according to the succession of the assembly. To get the assembly commands for the robot the command string from the placement name (Table 1) has to be interpreted and broken down to commands for the robot (section Robotic Arm, Gripper, Sensors and Tools). As programming paradigm, we used skill primitives, with which we divided the assembly tasks in subtasks.

Discussion

A complete workflow from product design through assembly development to automated assembly has been implemented and tested. The aims pursued were in order of importance

1. blend in with existing product development workflows,
2. blend in with existing workplaces designed for humans,
3. be flexible and allow for assembly of a large variety of products.

To blend in with existing workflows it was sought to link directly the most common tool for product design and development (the CAD software) and the most common tool for automated assembly (the industrial robot with its control software). Both have been linked through an additional piece of software, a program written in C#. This requires the assembly development to take place within the CAD environment. As such this solution targets companies, who do not perceive this requirement as limiting, and hence it is certainly suited for smaller companies, which do have rather simple processes for assembly development.

The solution employs the placement name of Solid Edge and its member structure, to store the information, which was generated during assembly development. As such it depends on Solid Edge, though it can easily be ported to other CAD tools if the necessary interfaces are available. The solution shows a simple way to augment the raw CAD file with information on how to assemble the unit. It also shows a possible way how tools can be used, which is one requirement if the robot should be able to blend in with workplaces for humans. In the current solution the use of tools is controlled by the corresponding key-value-pair in the placement name. How the tool is used is hard coded in the program. Only the use of a screwdriver has been implemented.

Valuation from industrial partners has been positive. Deleting parts from the CAD assembly and rerun the program will result in the robot not taking up that part during the next assembly procedure. Moving the part to another location will result in the robot picking up that part at another location or performing the joining steps at another location, which will work when the other joining parts are prepared for the new location or bring the system to an error state if for example the fitting is at the wrong location. There are no limits other than those of the robot and the fact that only a limited number of joining operations are already implemented. Likewise, the speed of the assembly procedure is only limited by the usual safety aspects and the speed of the robot. The program execution to extract the data from the CAD and to generate the assembly steps happens virtually instantly.

An important aspect is the skill primitive nets. The level of abstraction of the instruction which can be given as instruction in the tree structure, depends on the implemented skills. With the current implemented skills, the assembly of the gearbox can be accomplished, and expected tolerances can be overcome, however, the instructions for the assembly have to be laid out on a very low level. A more extensive skill set would allow for a more comfortable assembly development experience.

Concerning the flexibility in general, the current solution shows where the biggest open issues are to find. These are most of all gripping issues. In the current solution three pneumatic grippers with fingers with positive-locking grip each dedicated to a particular part are installed. This ensures safe grip and precise positioning for all projected parts, but fails to handle parts, which deviate from

what has been projected by the time of finger design. As alternatives to positive-locking grip regripping (Tajima et al. 2020), visual servoing (Watson et al. 2020), haptic feedback (Chin et al. 2019) and novel gripper configurations (Angelini et al 2020) may be considered. How these can be combined to offer efficient new skills needs to be investigated.

Conclusions

With the proposed software, a robot can perform an assembly without the need for being programmed. In the case of the gripper and parts considered here, a collaborative robot could perform the assembly without fences, however a non-collaborative robot behind fences would be able to perform the assembly faster. The assembly development is carried out by the product designer and not by the robot or its controller. As such the operator still has full control over the assembly process without the need to be trained in robot programming. For a comprehensive control of the robot's movements, alternate assemblies have been used to specify intermediate positions. These proved to be a viable way to avoid collisions and reach the right positions before inserting axes, screws, and other parts, which have to be inserted from a defined angle.

Furthermore, during assembly development no further software or tools are used than the CAD software and the program presented here. This is a first step in making the robots blend in better in existing work processes. With a more versatile set of skill primitives, other types of input sources might be considered. Especially documents in human readable format could boost acceptance of robots SMEs.

The flexibility of the solution is limited by the positive locking grip, which was adopted to reach the precision necessary for the peg-in-hole and gearwheel-aligning tasks. Hence, to improve the method, the research focus on that subject should be intensified.

References

Angelini F, Petrocelli C, Catalano MG, Garabini M, Grioli G, Bicchi A (2020) SoftHandler: an integrated soft robotic system for handling heterogeneous objects. *IEEE Robotics & Automation Magazine* 27(3): 55–72.

Chin L, Yuen MC, Lipton J, Trueba LH, Kramer-Bottiglio R, Rus D (2019) A simple electric soft robotic gripper with high-deformation haptic feedback. In *2019 International Conference on Robotics and Automation (ICRA)*, 2765–2771.

Cserteg T, Erdős G, Horváth G (2018) Assisted assembly process by gesture controlled robots. In *Procedia CIRP*, 51–56.

F&P Robotics (2018a) *Git repository for myP additions to ROS*. Retrieved from: https://github.com/fp-robotics/myp_ros. [Accessed 18 February 2021]

F&P Robotics (2018b) *myP Script Functions Manual Version 1.3.2*. Glattbrugg, Switzerland.

Linnerud ÅS, Sandøy R, Wetterwald LE (2019) CAD-based system for programming of robotic assembly processes with human-in-the-loop. In *2019 IEEE 28th International Symposium on Industrial Electronics (ISIE)*, 2303–2308.

Markis A, Montenegro H, Neuhold M, Oberweger A, Schlosser C, Schwald C, et al. (2016) *Sicherheit in der Mensch-Roboter- Kollaboration*. (Safety in human-robot collaboration). Wien.

Michniewicz J, Reinhart G, Boschert S (2016) CAD-based automated assembly planning for variable products in modular production systems. In *Procedia CIRP*, 44, 44–49.

Mišeikis J, Caroni P, Duchamp P, Gasser A, Marko R, Mišeikiene N, et al. (2020) Lio-A personal robot assistant for human-robot interaction and care applications. *IEEE Robotics and Automation Letters* 5(4): 5339–5346.

Perzylo A, Nikhil S, Profanter S, Kessler I, Rickert M, Knoll A (2016) Intuitive instruction of industrial robots: semantic process descriptions for small lot production. In *2016 IEEE/RSJ International Conference on Intelligent Robots and Systems (IROS)*, 2293–2300.

Perzylo A, Rickert M, Kahl B, Somani N, Lehmann C, Kuss A, et al. (2019) SMErobotics: Smart robots for flexible manufacturing. In *IEEE Robotics & Automation Magazine* 26(1): 78–90.

Schmidbauer C, Komenda T, Schlund S (2020) Teaching cobots in learning factories - User and usability-driven implications. *Procedia Manufacturing* 45(Apr): 398–404.

Siemens Product Lifecycle Management Software Inc. (2011) *Alternate assemblies*. Retrieved from: http://support.industrysoftware.automation. siemens.com/training/se /en/ST4/pdf/spse01685-s-1040_en.pdf. [Accessed 19 February 2020]

Tajima S, Wakamatsu S, Abe T, Tennomi M, Morita K, Ubata H, et al. (2020) Robust bin-picking system using tactile sensor. *Advanced Robotics* 34(7–8): 439–453.

Thomas U, Finkemeyer B, Kroger T, Wahl FM (2003) Error-tolerant execution of complex robot tasks based on skill primitives. In *Proceedings - IEEE International Conference on Robotics and Automation* 3, 3069–3075.

Thomaz AL, Breazeal C (2008) Teachable robots: understanding human teaching behavior to build more effective robot learners. *Artificial Intelligence* 172(6–7): 716–737.

Transeth AA, Stepanov A, Linnerud ÅS, Ening K, Gjerstad T (2020) Competitive high variance, low volume manufacturing with robot manipulators. In *2020 3rd International Symposium on Small-scale Intelligent Manufacturing Systems (SIMS)*, 1–7.

Tsarouchi P, Athanasatos A, Makris S, Chatzigeorgiou X, Chryssolouris G (2016) High level robot programming using body and hand gestures. *Procedia CIRP* 55(Dec): 1–5.

von Drigalski F, Schlette C, Rudorfer M, Correll N, Triyonoputro JC, Wan W, et al. (2020) Robots assembling machines: learning from the World Robot Summit 2018 Assembly Challenge. *Advanced Robotics* 34(7–8): 408–421.

Wang L, Gao R, Vánca J, Krüger J, Wang X, Makris S, et al. (2019a) Symbiotic human-robot collaborative assembly. *CIRP Annals* 68(2): 701–726.

Wang T, Li D, Liu X, Zhou X (2019b) Gesture control for human-robot interaction based on three-way decision model. In *2019 IEEE 16th International Conference on Networking, Sensing and Control (ICNSC)*, 311–316.

Warfield B (2020, September 22) *CNCCookbook 2016 CAD survey results, part 1: market share - CNCCookbook: be a better CNC'er*. CNC Cookbook.

Watson J, Miller A, Correll N (2020) Autonomous industrial assembly using force, torque, and RGB-D sensing. *Advanced Robotics* 34(7–8): 546–559.

Athens Journal of Technology and Engineering - Volume 9, Issue 1, March 2022 – Pages 25-42

Compact Shaft-Rotating Swerve Drive with Prong Structure for Highly-Maneuverable and Agile Robots

By Miles Vranas[*] *& Nikos J. Mourtos*[±]

Robots are becoming increasingly important in our lives. Although many robots are stationary, for example robotic arms, moving robots are of particular interest for many applications. Applications of moving robots today include combating COVID-19 in hospitals, transporting goods in and across warehouses and distribution centers, and moving equipment and instrumentation in space, to name a few. Mobile robots are often required to maneuver rapidly in tight spaces. The best way to achieve this is through a modular assembly called Swerve Drive, which is a driven wheel that can pivot 360 degrees. Three or more modules can be placed at the corners of the robot, allowing high levels of maneuverability, such as, for example, spinning while following a path in any direction. This paper presents the design of a swerve drive module, which improves the current state-of-the-art. The proposed Swerve Drive module has similar properties to current designs available in the market in four out of six metrics defined in this work, while it does significantly better in the other two metrics.

Keywords: *robotics, mechanical engineering, drivetrain, maneuverability, mobile, swerve-drive*

Introduction: The Need for Swerve Drive

In today's society, moving robots are becoming increasingly important in many applications (Carothers 2014). As machine learning and artificial intelligence become more advanced, mobile robots are able to take on increasingly important tasks. With this advancing technology, a more advanced robot drivetrain is needed to allow robots to operate quicker, more efficiently, and in much smaller spaces. Most drivetrains today operate like tanks or cars. However, Swerve Drive (Swerve Drive Specialties 2021), is dramatically different. It is able to maneuver in ways that no other drivetrain can.

Swerve Drive is a modular assembly, which consists of a driven wheel (blue) and a base, which rotates around the vertical axis running through the center of the wheel. There are two motors, one which drives the blue wheel, and the other which pivots the direction in which the wheel is facing. In Figure 5, the base which rotates around the vertical axis can be seen as well. A robot which utilizes Swerve Drive would typically contain four Swerve Drive modules. A depiction of such a drivetrain is shown in Figure 1, for illustration purposes. Other configurations are possible, such as a drivetrain which utilizes three Swerve Drive modules, or more. This

[*]Mechanical Engineer, Monte Vista Robotics Team, USA.
[±]Professor and Chair, Aerospace Engineering, San Jose State University, USA.

allows a robot which utilizes Swerve Drive to spin while moving along any designated path. Each wheel can rotate while at the same time pivoting along the vertical axis. This arrangement allows for increased maneuverability.

Figure 1. *Bottom (left) and Top (right) Views of a Drivetrain Utilizing Four Swerve Drive Modules*

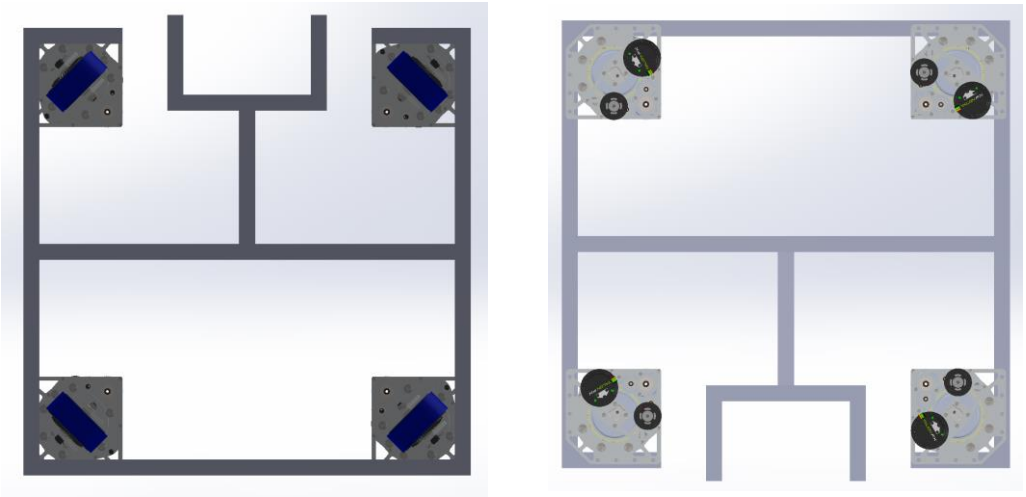

Figure 2 shows paths of a robot using Swerve Drive. As can be seen, the Swerve Drive allows for a better-than-human maneuverability in the given environment.

Figure 2. *A Schematic of the Paths and Orientations of a Swerve Drive Robot (green indicates the path, red indicates direction in which the robot is facing, white indicates the position of the robot)*

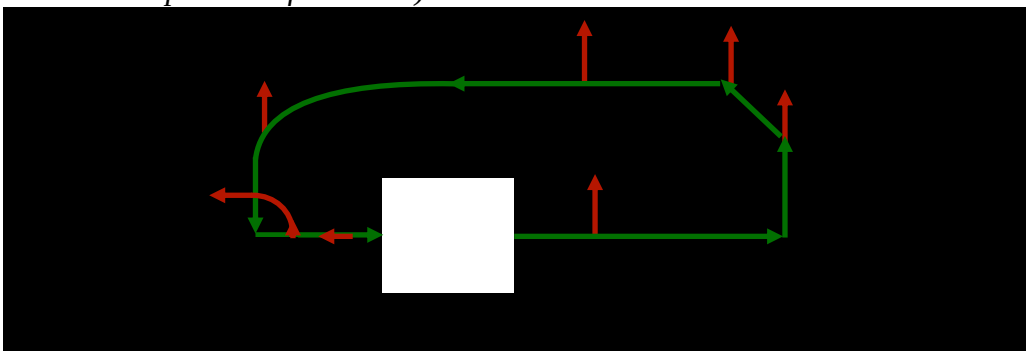

Mobile robots are used to combat COVID-19 (Seidita et al. 2021, Ackerman 2020, Cardona et al. 2020), help healthcare workers in hospitals (Melanson 2018, Bloss 2011), transport goods in and across warehouses and distribution centers (Dunakin 2020, Simon, 2019), in space programs (NASA Technology Transfer Program, Mars 2020 Mission Perseverance Rover), as well as for specific functions in stores (Ciment 2020), to name a few applications. Swerve Drive designs are already in use today (Swerve Central 2021), however, their operation and capabilities allow much room for improvement. This paper presents the design of a Swerve Drive module with improved characteristics.

Background Review

Many Swerve Drive robots rely on chains or belts (Swerve Drive Specialties, 2021), which can lose tension with time, causing loss in precision or total failure. Some designs, such as those by Westcoast Products (Westcoast Products, 2021), do not require belts. However, they do require specialized machines, such as high-end CNC mills (Tormach 2021, Stepcraft, 2021) and hobbing machines (Lieherr 2021) to produce intricate gears. This increase difficulties and cost in the manufacturing process. Furthermore, existing Swerve Drive modules do not have the encoder placed directly on the rotating wheel mount because of restrictions caused by the placement of components (see for example Westcoast Products 2021), causing poor directional precision. In the proposed design all these issues are resolved, while maintaining low-price, small size, low weight, and structural integrity. In Table 1, the characteristics of the best current state-of-the-art Swerve Drive (Westcoast Products 2021) is listed for comparison.

Methodology

Design Criteria and Constraints

Design criteria and constraints were explored in Solidworks (Dassault Systems 2021) and are described below, along with a scoring system that is used in Table 1 to compare the proposed design with the current state-of-the art.

Price for each Swerve Drive module was explored using existing parts from sources such as McMaster Carr (2021) and stock material, such as 6061 0.25" aluminum sheets. The target price of each module is set at $ 650.00, below the price of the current state-of-the-art, which is $685.37, including all necessary options (Westcoast Products 2021).

Scoring for price:

+10 points if $650 or lower
-1 point for every $50 over $650

Manufacturability expresses the ease of manufacturing and is determined by the number of parts in a single module, as well as the need for specialized manufacturing machines.

Scoring for manufacturability:

+5 points if number of parts is 200 or less; -0.5 point for every 20 parts over 200
+5 points if special equipment worth more than $5000 is not necessary to manufacture any part of the module; +0 points otherwise

Overall size is determined by the size of the wheel and motors. The target size for each module is set at a length of 6", a width of 6", and an overall height (from

the bottom of the wheel to the top of the motor) of 10". This size is less than that of the current state-of-the-art (Westcoast Products 2021).

Scoring for size:

+1 for each 4" less than 44" of the perimeter (max 5 points)
+0 if perimeter is greater than 44"
+1 if height is 1" less than 15" (max 5 points)
+0 if height is greater than 15"

Weight is determined by the weight of the two motors and the wheel, which is approximately 2.5 pounds. The target weight for each module is set to approximately three times that amount or 7.5 pounds.

Scoring for weight:

+1 point for each pound less than 15
+0 points if module weighs 15 pounds or more

Structural Integrity refers to the ability of the module to operate under load. The target criteria are as follows: (a) module can be lifted off the ground without separating, (b) module can operate without falling apart, (c) moving parts operate properly under load, and (d) four modules can support a robot weight of at least 160 pounds.

Scoring for structural integrity:

+2.5 module can be lifted off of the ground without separating
+2.5 module can operate without falling apart
+2.5 moving parts operate properly under load
+2.5 4 modules can support a robot weight of at least 160 pounds

Precision refers to the ability of the wheel to change direction accurately, as well as to the precision of the directional sensors. The first target is for the encoder to be directly mounted to the rotating wheel mount, so it will directly read the direction the wheel is facing. The second target is to avoid using belts or chains, as they become slacked, causing loss of precision.

Scoring for precision:

+5 encoder is directly mounted on the rotating wheel mount
+5 no belts or chains used

Iterations and Evaluations of Designs Using CAD Tools

Table 1 shows that the Swerve Drive module proposed here provides improved performance over the current state-of-the-art (Westcoast Products 2021), having similar properties in four out of six metrics, while doing significantly better in the other two.

Table 1. *The Given Scores are between 0 (Poor) and 10 (Perfect). A Score of 8 or Above (Marked as Green), Indicates a Sufficient Design*

Iteration	Price	Manufacturability	Size (L x W x H)	Weight	Structural Integrity	Precision	Figure Number
1	6.48/10 ($826.55)	8.45/10 (Number of parts is 262, no machines over $5000 are needed to manufacture any part of the module)	3.53/10 (7.94"x9"x14")	4.73/10 (10.27 pounds)	10/10 (Module is able to be lifted off of the ground without separating, can operate without falling apart, moving parts operate properly under load, and 4 modules can support a robot weight of at least 160 pounds)	0/10 (Encoder is not directly mounted to rotating wheel mount, chains used)	2
2	6.00/10 ($850.94)	9.4/10 (Number of parts is 223, no machines over $5000 are needed to manufacture any part of the module)	3.5/10 (8.5"x8.5"x14")	4.26/10 (10.74 pounds)	5/10 (Module is able to be lifted off of the ground without separating, can operate without falling apart, moving parts do not operate properly under load, and 4 modules cannot support a robot weight of at least 160 pounds)	10/10 (Encoder directly mounted to rotating wheel mount, no belts or chains used)	3
3	8.90/10 ($705.61)	10/10 (Number of parts is 186, no machines over $5000 are needed to manufacture any part of the module)	7.72/10 (5.93"x5.93"x12.28")	9.25/10 (5.75 pounds)	10/10 (Module is able to be lifted off of the ground without separating, can operate without falling apart, moving parts operate properly under load, and 4 modules can support a robot weight of at least 160 pounds)	10/10 (Encoder directly mounted to rotating wheel mount, no belts or chains used)	4

Iteration	Price	Manufacturability	Size (L x W x H)	Weight	Structural Integrity	Precision	Figure Number
Final (4th)	10/10 ($649.07)	10/10 (Number of parts is 189, no machines over $5000 are needed to manufacture any part of the module)	10/10 (5.95"x5.95"x9.72")	8.67/10 (6.33 pounds)	10/10 (Module is able to be lifted off of the ground without separating, can operate without falling apart, moving parts operate properly under load, and 4 modules can support a robot weight of at least 160 pounds)	10/10 (Encoder directly mounted to rotating wheel mount, no belts or chains used)	5
Best current state-of-the-art (Westcoast, 2021)	9.3/10 ($685.37)	5/10 (Number of parts is 153, machines over $5000 are needed to manufacture multiple parts of the module)	10/10 (5.5"x5.5"x9.6")	9.5/10 (5.5 pounds)	10/10 (Module is able to be lifted off of the ground without separating, can operate without falling apart, moving parts operate properly under load, and 4 modules can support a robot weight of at least 160 pounds)	0/10 (Encoder is not directly mounted to rotating wheel mount, belts used)	

Design Iterations

A brief description of the various design iterations is given below.

Iteration 1 (Figure 3)

The first functional Swerve Drive design is presented in Figure 3. This design utilizes a planetary gearbox, with an encoder mounted to it, to reduce rotational velocity and thus achieve better precision. Furthermore, it uses a chain to transfer torque from the gearbox to the pivoting wheel structure. A reduced rotational velocity is needed to drive the wheel in this configuration, as a result of using standard gears; the torque is transferred from the motor to a central shaft, which drives bevel gears. The gears power a chain, which then drives the wheel. 90° brackets are used to connect the horizontal and vertical structural members of the pivoting structure. Lastly, a turntable is used to connect the bottom and top structures together, and to allow rotation between the two structures.

Figure 3. *Images from the First CAD Iteration of the Swerve Drive*

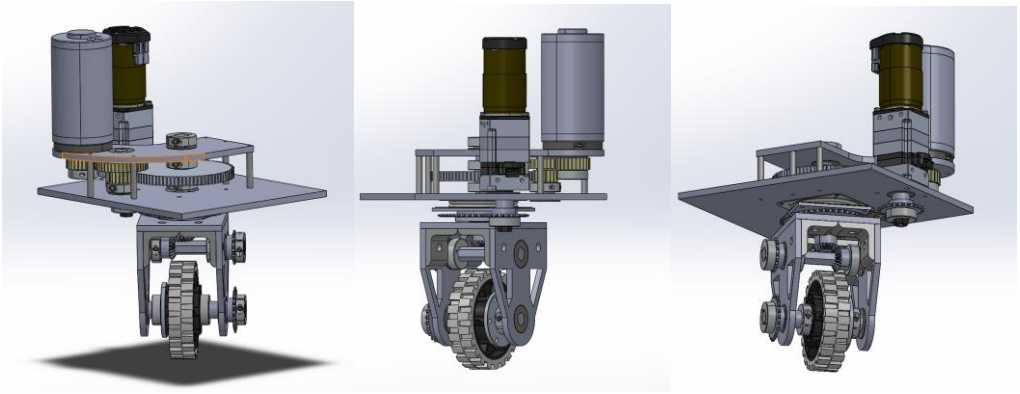

Iteration 2 (Figure 4)

Improving upon the first iteration, chains are replaced by a planetary gearbox directly above the bottom structure, which applies torque to a shaft mounted to the structure. The benefit of this gearbox placement is that the encoder is directly connected to the bottom structure, allowing a direct reading of the wheel direction. To drive the wheel, a motor powers a gear mounted onto the shaft, which pivots the bottom structure by placing a bearing in the center of the gear. Another gear is placed below the first one, and the torque is transferred between the two via a six-bolt circle. The bottom gear powers a shaft with a bevel gear on it, which transfers torque to a second bevel gear, directly powering the wheel. To accommodate for the new gear placement, a substantially larger turntable is used.

Figure 4. *Images from the Second CAD Iteration of the Swerve Drive*

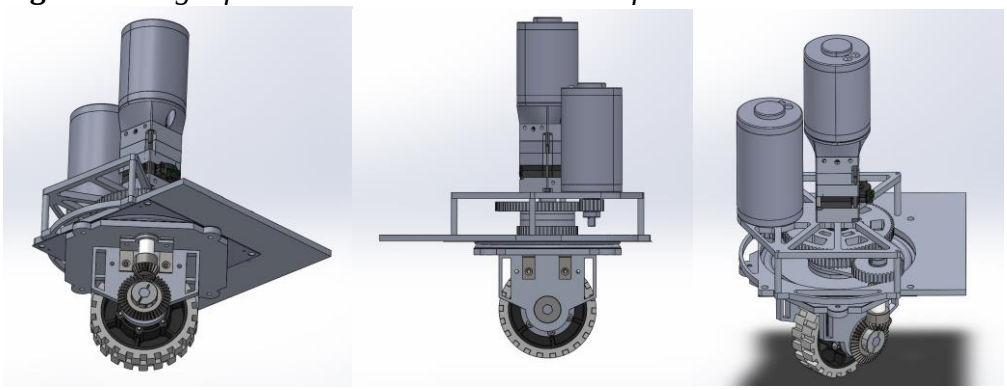

Iteration 3 (Figure 5)

Improving on the second iteration, the turntable is replaced by an "X-Contact" ball bearing (RBC Bearings 2021), which is held in place by a nut touching the outer ring on the top of the bearing, and a screw touching the same area on the bottom. X-Contact bearings have two contact points on the outer ring raceway, and two contact points in the inner ring raceway, in an X-pattern. This allows the bearing to

endure large vertical forces. Furthermore, the bearing is thin, allowing for the size of the module to be reduced substantially. In addition to the 90° brackets connecting the vertical and horizontal members of the pivoting structure, there is a "prong" structure, shown in Figure 6, and described in the "Description of the Final Design" section of this paper.

Figure 5. *Images from the Third CAD Iteration of the Swerve Drive*

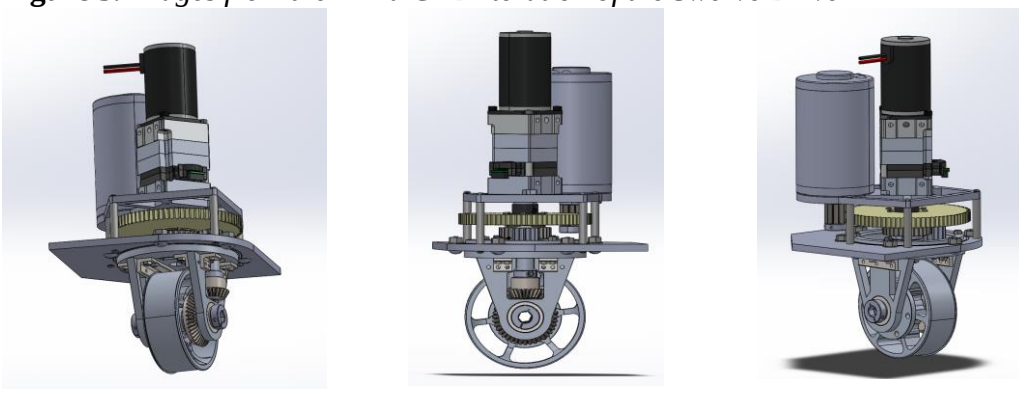

Iteration 4 (Figure 6)

Figure 6. *Different Views of the Fourth CAD Iteration and Final Swerve Drive Design*

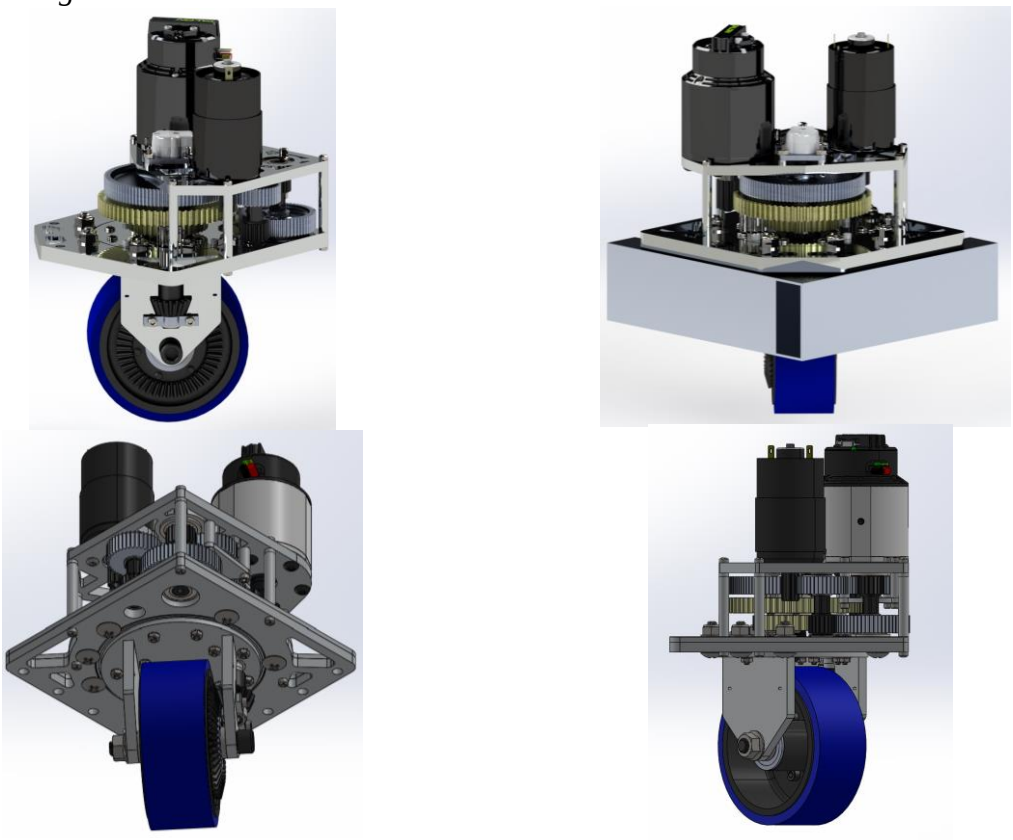

Improving on the third iteration, the planetary gearbox is replaced by normal gears. In this gear arrangement, the final pivoting gear is mounted onto a central shaft, just like the planetary gearbox in the third iteration. The vertical bevel gear is now supported below by a machined (using a CNC Mill) piece of 0.25" aluminum, which has holes to mount it to a vertical wheel support bracket. To add extra support allowing for the removal of the 90° brackets, holes are drilled into the top of the vertical wheel support brackets, which are then tapped using a hand tap allowing for a screw to secure the horizontal and vertical members of the structure together. To accommodate for the use of a spiral point tap, which pushes metal chips downwards, a small slot perpendicular to the hole is machined directly through the bracket, allowing for an exit for the chips from the hole.

Results

Description of the Final Design

Within the Swerve Drive there are two sub-mechanisms: a wheel pivoting mechanism, which changes the direction in which the wheel is pivoted, and a drive mechanism, which applies torque to the wheel. In this design, the drive mechanism is built around the wheel pivoting mechanism. The wheel pivoting mechanism is supplied torque by a 775 motor (Banggood 2021), which is small, lightweight, and relatively inexpensive. The motor has a maximum angular velocity of 21000 RPM, and there is a gear ratio of 50:1 between the pivoting structure and the motor, so the wheel can pivot at a maximum angular velocity of 420 RPM. This gear ratio was chosen to minimize the jitter caused by the DC motor, as well as any overshoot that may result from computational lag, while maximizing the angular velocity of the pivoting structure. To achieve this gear ratio, four-stages of gears were used and optimized to fit into the smallest possible volume. In Figure 7 each stage is represented by a box with the number of the stage next to it, and each gear is labelled with letters A-G, A being the first gear powered by the motor, and G being the last, which applies torque directly to the pivoting structure.

Stages 1 and 2 contain two gears on top of one another held in place by a retaining ring on a single hexagonal shaft. Gear F is not needed to achieve the 50:1 gear ratio, but due to the placement of gear E, it is needed to transfer torque between gears E and G. The placement of gear D prohibits the use of a shaft running from gear F directly to a bearing on the bottom of the module, so a floating piece of machined 0.125" aluminum, held in place by three standoffs, is utilized to securely hold a bearing below gear F, adding a second contact point for the shaft, securely holding the gear in place.

To transfer torque between gear G and the pivoting structure, a central shaft (black) is placed between the gear and the pivoting structure, as shown in Figure 8.

Figure 7. *Schematic of the Final Swerve Drive Design, Showing Four Stages of Gears and Each Individual Gear Used in the Wheel Pivoting Sub-Mechanism*

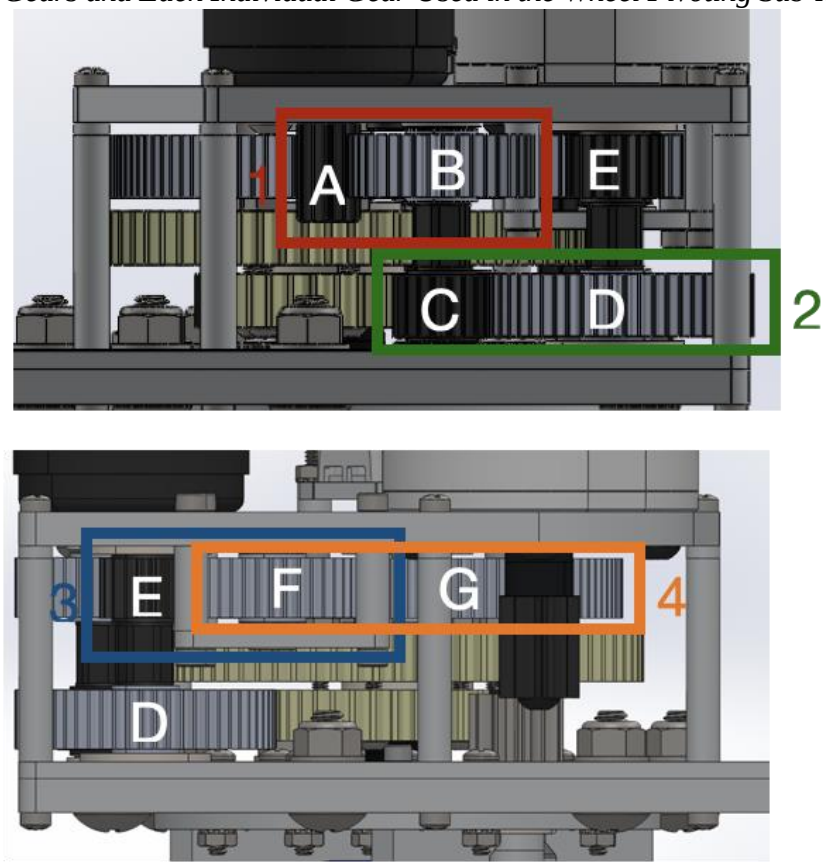

Figure 8. *Cross Sectional CAD Image of the Final Swerve Drive Design*

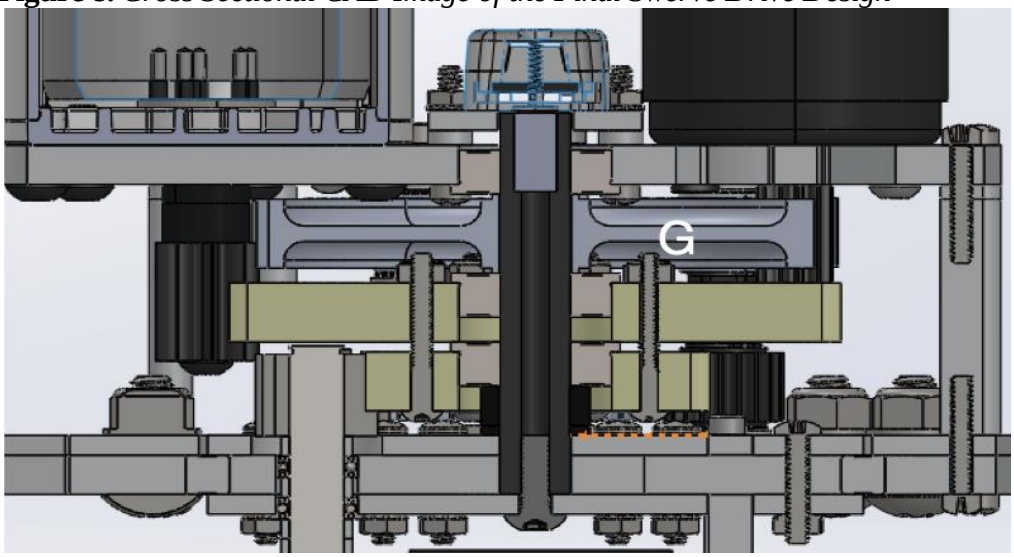

A polarized magnet is placed in this shaft, with an encoder directly above it to read the exact direction in which the wheel is pivoted. The encoder proposed for this design is (CTR CANcoder 2021). Please note that the encoder is only affected

by metal very close to it. The encoder is not affected by metal that is further than 0.116" away from it. Any steel frame that the module is mounted on would need to be substantially closer than 0.116" away from the encoder to affect the precision of its readings. The shaft is threaded on the bottom, using a hand tap such as a spiral point tap, to allow for a screw to secure the shaft to the bottom pivoting structure. The polarized magnet is held securely in place within the shaft using epoxy glue.

Built around this wheel pivoting mechanism is the drive mechanism, supplied torque by a 400-watt brushless motor (CTR Electronics 2021a, b) with a maximum rotational velocity of 6380 RPM, a stall torque of 3.46 ft-lbs, and a stall current of 257A. Depending on the application, different gear ratios for the drive mechanism may be used. In this application, a gear ratio of 6.44:1 is used, as it maximizes robot velocity at a theoretical maximum velocity of 17.26 feet/second, while allowing the robot to operate at full power for 3 minutes with an 18Ah 12V lead acid battery (Home Depot 2021a). To achieve this gear ratio, three-stages of gears are used. In Figure 9 each stage is represented by a box with the number of the stage next to it and each gear is labelled with letters A-F, A being the first gear powered by the motor and F being the last, which applies torque directly to the wheel.

Figure 9. *Schematic of the Final Swerve Drive Design Showing the Three Stages of Gears and Each Individual Gear In the Wheel Driving Sub-Mechanism*

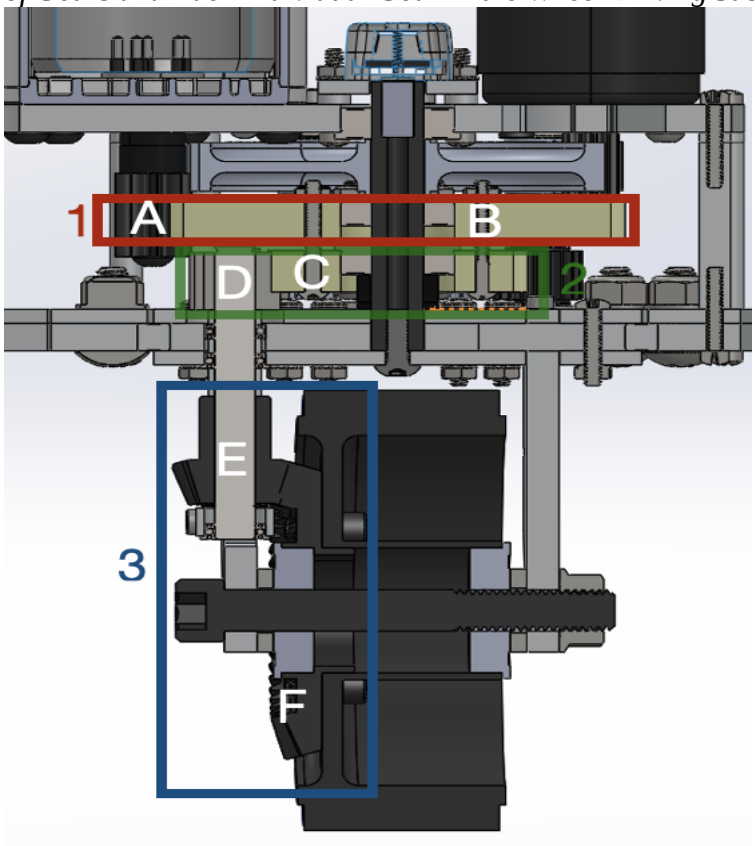

Stage 1 contains a pinion gear (A), mounted on the motor, which drives a spur gear (B). Stage 2 contains a large gear (C), driving a small gear (D). To connect

gears B and C, a 6-bolt circle is drilled into them using a vertical drill press (Home Depot 2021b). To ensure that all six holes are drilled into the gears precisely, a wooden "stencil" is machined using a CNC Mill (Stepcraft 2021). The stencil is held in the direct center of the gear using a small protrusion in the gear, which exists before the bearing bore is drilled. Using tape or glue, the stencil is then held in place rotationally, allowing for the holes to be drilled into the gear using the vertical drill press, with the wooden stencil as a reference. A bearing bore is then drilled into the center of the gears, so that bearings can allow for the hexagonal shaft, which pivots the bottom pivoting structure, to run through the gears. Gears B and C originally have a hexagonal bore, so that the drill bit for the bearing bore is placed so that it is tangent to all six sides of the hex bore. After the bearing bore and the six-bolt circle are drilled into the gears, a flanged bearing is placed so that its flange is above gears B and C individually. This allows gear G of the pivoting mechanism to be held securely in place above gear B of the drive mechanism. The flange of the bearing in gear C allows for a small gap between gears B and C, while holding gear B in place above gear C. Plastic spacers below the bearing of gear C keep both gears C and B in the correct position on the hexagonal shaft. Six nuts and bolts placed through the six-bolt circle of the gear, with space for the nuts above gear B resulting from a pocket, made by the manufacturer in gear G of the pivoting mechanism, hold securely gears B and C together. Next, gear D is held securely in place on a key shaft with a retaining ring above and custom 0.125" aluminum spacers below. There is space for the retaining ring above gear D because the flange in the bearing of gear C makes a gap between gears B and C. A key in gear D allows the gear to apply torque to the key shaft which drives gear E. To achieve the proper gear ratio, and to transfer rotation around the vertical axis of the key shaft to the horizontal axis, which the wheel rotates around, two bevel gears are used in stage 3. Torque can be applied on gear E by a key running through a key shaft. Gear E then applies torque to gear F, which is held securely in place on the wheel using a six-bolt circle on both the wheel and the gear. The six-bolt circle on gear F is tapped by the manufacturer, allowing for six bolts to hold the gear and the wheel securely in place. This allows the module to drive a 4" diameter wheel.

To structurally support the pivoting and drive sub mechanisms a framework utilizing standoffs, nuts and bolts, and 0.125" and 0.25" aluminum components was machined using a sub-$5000 CNC Mill (Stepcraft 2021) and was tapped/threaded using various types of manual taps, including spiral point taps. Figure 10, shows the key innovative aspects of the Swerve Drive structure, which allow the module to be manufactured with a sub-$5000 CNC Mill (Stepcraft 2021).

Image 1 in Figure 10 shows the entire structure, which includes the upper and lower portions of the module, while image 2 shows the upper structure. Circled in red are the module mount plates which consist of 0.25" and 0.125" thick aluminum plates bolted to one another using 0.25" diameter bolts and nylon insert locknuts. The central circle of the 0.125" module mount plate is slightly smaller in diameter than that of the 0.25" module mount plate, so that the 0.125" plate has a contact point with the top of the outer ring of the central X-Contact bearing (RBC Bearings 2021). This bearing connects the upper and lower structures, while allowing

rotational movement between the two to ensure that a vertical force applied to the wheel and the lower structure is safely transferred to the robot.

Using standoffs and bolts, the motor mount plate, circled in black in image 2, is securely attached to the module mount plates. The motor mount plate has holes to allow for the motors of the drive and pivoting sub-mechanisms to mount securely to the plate. Holes in both the module mount plate and the motor mount plate, machined using a CNC Mill (Stepcraft 2021), accommodate the bearings which support the shafts of the pivoting and drive mechanisms. Circled in green in image 2 is the encoder mount, which is a floating piece of 0.125" thick of aluminum, held in place with four standoffs, four screws, and four locknuts. The encoder is placed on this component to allow placement of the bearing that supports the central shaft, which pivots the lower pivoting structure. Because the encoder is a magnet encoder, all components close to it, including the mount, are made of aluminum.

In image 3 the X-Contact bearing and seven bolts with their heads touching the outer ring of the bearing are circled in orange. These bolts ensure that if the module is lifted off of the ground, the upper and lower structures do not detach from each other. Furthermore, if uneven forces are applied on the circumference of the bearing, both sides of the bearing will stay in place. Image 4 shows the floating structure, which holds the shaft of gear F of the pivoting mechanism in place, circled in blue. This structure, machined using a CNC Mill, consists of 0.125" aluminum with a hole for a bearing in the center and holes for three screws which connect to three standoffs to the motor mounting plate.

Image 5 shows the lower structure. The red and blue arrows point to two 0.125" aluminum plates placed above and below the X-Contact bearing. Going through these plates are prongs protruding from the top of the wheel supports, shown by black and orange arrows in the figure. In these prongs are rectangular holes, which are circled in red in image 7. "Sandwiched" between the two 0.125" aluminum plates placed above and below the X-Contact bearing are 3 components, labelled A-C in image 6. Going through components A and C are the wheel supports, labeled D and E in image 6. Going through the rectangular hole in the prong of component D is component A, which has a prong of its own and screws, which run through the two 0.125" aluminum plates and itself. Component A is circular on the outside, with a radius matching the inner ring of the X-Contact bearing and placed inside the inner diameter of the bearing. To allow the key shaft and bevel gear to run through it, component E has two prongs with rectangular holes in them. Running through these rectangular holes are the two prongs of component C, which is supported by screws running through the aluminum plates above and below the bearing.

Component C, like A is also designed to be placed inside the inner diameter of the bearing. Component B is placed between components A and C with a bore in the center for the hexagonal shaft that rotates the bottom pivoting structure. In image 7, a hole running through components E and component D is circled in orange. This hole, threaded to allow for a screw to run from the 0.125" aluminum plate above the X-Contact bearing through components D and E, adds extra support to the wheel. To allow for this hole to be threaded by a tap that is not

meant for blind holes, such as a spiral point tap, a small oval-shaped hole, circled in black in image 7, was machined horizontally through components D and E using a CNC Mill. This hole allows for the metal chips "produced" by the tap to escape through the bottom of the hole, ensuring that the hole is properly threaded and the tap does not fail.

In image 8, two flanged ball bearings are circled in blue and green. The flanged bearing circled in green is supported below by component E using small flanges circled in red, touching the outer ring and flange of the bearing. The flanged bearing circled in blue in image 9 is supported below by a flange (also circled in blue), which touches the outer ring and flange of the bearing. The bearing is supported above by a 0.25" piece of aluminum machined using a CNC Mill. This component has a ring shape in the center to support the bearing and two portions on either side, which stick out and have a horizontal hole drilled into them using a drill press. These holes accommodate screws, which go into holes machined into component E, circled in red in image 9. The holes in component E are also tapped to allow for the bearing support to be held securely in place.

Figure 10. *The final Swerve Drive Design*

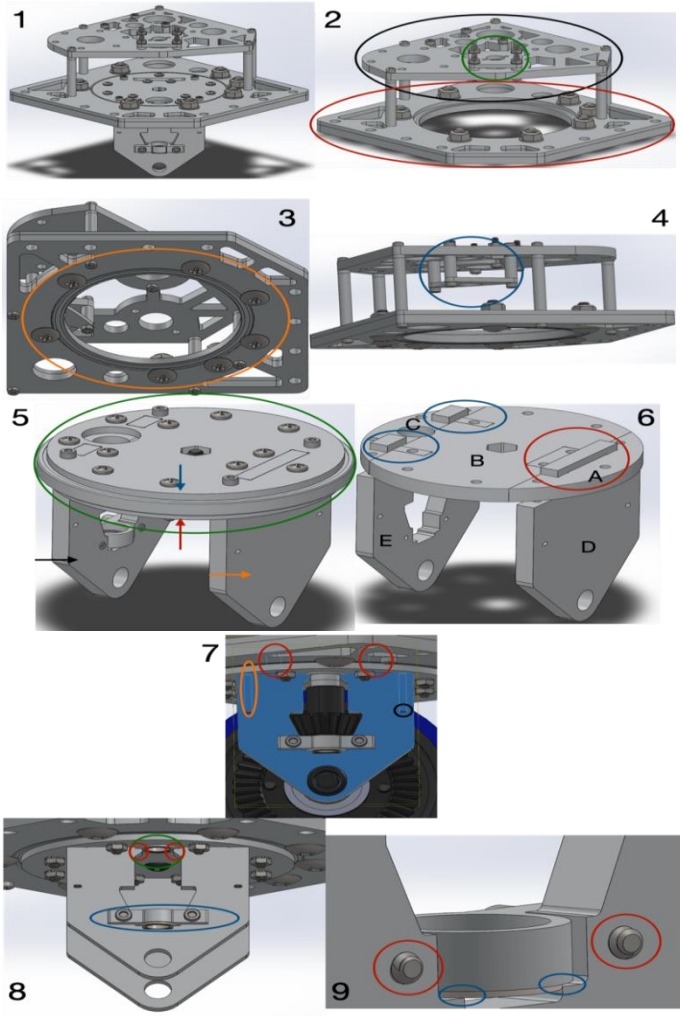

Building and Testing a Physical Prototype

Since the CAD of the Swerve Drive module is now complete, a prototype module can be manufactured. The silver components shown in Figure 8 are made of 1/8" and 1/4" aluminum which can be machined using a CNC Mill. All other components (i.e., gears, spacers, etc.) can be purchased directly from distributors like McMaster Carr (McMaster-Carr 2021). Unfortunately due to the Covid-19 Pandemic the metal components required to make the Swerve Drive module could not be bought or manufactured.

Figure 11. *Several Images of the Prototype Swerve Drive Module, Along with the Images of the Dolly Swerve Drive Prototype Assembly*

All components were manufactured with an Ender 3 Pro 3D printer (Creality 2021), with the exception of screws, standoffs, and spacers, which were purchased online (McMaster-Carr 2021). Thus a working prototype was built. To demonstrate functionality the motors for the module were connected to electronic speed controllers (ESCs), which were then attached to the receiver and transmitter of a remote-control car. For a fully functioning robot, the motors would have been controlled by an onboard computer. However, this was beyond the scope of this prototype, which was to manufacture a single Swerve Drive module prototype. Hence a dolly was constructed out of wood and four caster wheels and the Swerve Drive module was placed in the center of it. Using the remote control, it was possible to demonstrate the functionality of the Swerve Drive module prototype. The acceleration and turn speed of the module were exceptional. The structure was able to pivot 360 degrees around the vertical axis in less than one-second, while the wheel spun at more than 3,200 rotations per minute. In Figure 11, several images of the prototype Swerve Drive module, along with the images of the dolly Swerve Drive prototype assembly are shown.

Discussion

In the final Swerve Drive design, a DC motor with a 50:1 gear ratio, along with an encoder, is used to pivot the structure about the vertical axis. This setup offers exceptional accuracy and rotational velocity, and although is lighter, cheaper, and smaller than the best current state-of-the-art option (Westcoast Products 2021), it can still be improved. For example, in a future project, the pivoting motor could be replaced by a stepper motor (Pololu Robotics & Electronics 2021). This would eliminate the need for some gears, the DC motor, and the encoder, making the module lighter, smaller, and cheaper.

Conclusions

This paper presented the design of an advanced Swerve Drive module. Swerve Drive is a modular assembly, which consists of a driven wheel and a base that rotates symmetrically around the vertical axis running through the center of the wheel. There are two motors, one which drives the wheel, and the other which rotates the base around the vertical axis. This allows a robot which utilizes Swerve Drive to spin while moving along any designated path. A robot which utilizes Swerve Drive would typically contain four Swerve Drive modules. Each wheel can rotate while at the same time pivoting along the vertical axis. This configuration allows a high level of robot maneuverability.

A prototype was also manufactured using a 3D printer. The prototype verified the mechanical functionality of the proposed design, according to the design criteria and constraints set in the paper. The designed Swerve Drive module has similar properties to the best current design in four out of six metrics, while it does

significantly better in the other two out of six metrics, thus establishing this design as the new state-of-the-art.

In our current society, mobile robots are used to combat COVID-19 in hospitals, the transportation of goods in and across warehouses and distribution centers, in space programs, as well as in specific functions in stores, to name a few applications. The Swerve Drive design described here will help with the advancement of autonomous mobile robots. This advancement will allow autonomous mobile robots to be used in many more tasks in today's world.

References

Ackerman E (2020, March 11) *Autonomous robots are helping kill Coronavirus in hospitals*. Available at: https://bit.ly/3Ji048c.

Banggood (2021) *775 motor*. Available at: https://bit.ly/3BiqHqV.

Bloss R (2011) Mobile hospital robots cure numerous logistic needs. *Industrial Robot* 38(6): 567–571.

Cardona M, Cortez F, Palacios A, Cerros K (2020) Mobile robots application against Covid-19 pandemic. In *2020 IEEE ANDESCON*, 1–5.

Carothers J (2014) *Design of a triple singularity drive for mobile wheeled robots*. BSME Thesis. Department of Mechanical Engineering, Massachusetts Institute of Technology.

Ciment S (2020, January 13) *Walmart is bringing robots to 650 more stores as the retailer ramps up automation in stores nationwide*. Insider.

Creality (2021) *Ender 3 pro 3D printer*. Available at: https://www.creality3dofficial.com/products/creality-ender-3-pro-3d-printer.

CTR Electronics (2021a) *Falcon 500 motor*. Available at: http://www.ctr-electronics.com/talon-fx.html.

CTR Electronics (2021b) *CANcode*r. Available at: https://store.ctr-electronics.com/cancoder/.

Dassault Systems. (2021) *Solidworks*. Available at: https://www.solidworks.com/.

Dunakin C (2020, August 28) *5 ways autonomous mobile robots are transforming warehouses*. Available at: https://6river.com/how-autonomous-mobile-robots-are-transforming-warehouses/.

Home Depot (2021a) *18 Ah 12 volt lead acid battery*. Available at: https://www.homedepot.com/p/MIGHTY-MAX-BATTERY-12-Volt-18-Ah-Sealed-Lead-Acid-SLA-Rechargeable-Battery-ML18-12/308036944.

Home Depot (2021b) *Floor standing drill press*. Available at: https://www.homedepot.com/p/Jet-1-HP-15-in-Floor-Standing-Drill-Press-6-Speed-115-230-Volt-J-A3816-354500/ 204357268.

Lieherr (2021) *Gear hobbing machine*. Available at: https://bit.ly/3rLTfG0.

Melanson T (2018) *Mobile robots and COVID-19 – Helping healthcare workers*. Blog AP, Blog EU, News, News AP, News EU.

Mars 2020 mission perseverance rover: wheels and legs. Available at: https://mars.nasa.gov/mars2020/spacecraft/rover/wheels/.

McMaster-Carr (2021) Available at: https://www.mcmaster.com/.

NASA Technology Transfer Program (n/a) *Modular Robotic Vehicle (MRV)*. Available at: https://technology.nasa.gov/patent/MSC-TOPS-74.

Pololu Robotics & Electronics (2021) *Stepper motors*. Available at: https://www.pololu.com/category/87/stepper-motors.

RBC Bearings (2021) *X-contact bearing description*. Available at: https://bit.ly/3HM9VmB.

Seidita V, Lanza F, Pipitone A, Chella A (2021) Robots as intelligent assistants to face COVID-19 Pandemic. *Briefings in Bioinformatics* 22(2): 823–831.

Simon M (2019, June 5) *Inside the Amazon warehouse where humans and machines become one*. Wired, Science.

Stepcraft (2021) *D.840 Mill & Carve CNC package*. Available at: https://www.stepcraft.us/shop/product/70012-d-840-mill-carve-cnc-package-755?search=840.

Swerve Central (2021) Available at: https://team1640.com/wiki/index.php/Swerve_Central.

Swerve Drive Specialties (2021) *Specialties module*. Available at: https://www.swervedrivespecialties.com/products/mk3-swerve-module.

Tormach (2021) *PCNC 440CNC mill*. Available at: https://tormach.com/pcnc-440-starter-package.html.

Westcoast Products SS Swerve (2021) Available at: https://www.wcproducts.com/.

Athens Journal of Technology and Engineering - Volume 9, Issue 1, March 2022 – Pages 43-60

Effect of Borax and Boric Acid on Thermal and Flammability Properties of Rice Husk Reinforced Recycled HDPE Composite

By C. D. C. Dolotina[*] & Luis Maria T. Bo-ot[±]

Studies show Rice Husk (RH) and plastic appear viable in the production of a composite material. Flammability is a crucial parameter that limits multiple applications of such materials. Borax (BX) and Boric Acid (BA) have been used for wood and coating products, continually proving to be decent fire retardant agents in wood and plastic composites. In this study, the aim is to develop, test and investigate the thermal and flammability properties of RH reinforced Recycled High-Density Polyethylene (rHDPE) integrated with Maleic Anhydride Polyethylene (MAPE) as a binding agent, with Borax (BX) and Boric Acid (BA) as a fire retardant agent. RH was impregnated with BX and BA (1:1) solution at 2, 3, and 4% weight concentration and oven-dried after seven days at 105 °C for 24 hours. Only an average of 43 wt% of BX and BA remains after the impregnation process. Flammability test results show that adding RH to the composite enhanced flame retardancy compared to the pure rHDPE while adding MAPE as a binding agent makes the composite more flammable. Composite with BX and BA showed significant improvement in flame retardant properties by reducing the horizontal burning rate by 26% for 3% weight and 46% for 5% weight of MAPE. Thermogravimetric analyses exhibit an increase in the thermal stability by adding RH to reinforce rHDPE than pure rHDPE and further augmented by the integration of BX and BA.

Keywords: *rice husk, recycled high-density polyethylene, thermal, flammability*

Introduction

Rice Husk (RH) has been gaining attention as reinforcement in thermoplastic materials. Given the excellent compatibility between RH and the base polymer, RH would be an excellent option (Chand et al. 2010). Like any other natural fiber material, RH is hydrophilic and would result in poor compatibility and adhesion with the hydrophobic thermoplastic (Panthapulakkal et al. 2005). Silica, a silicon-cellulose membrane in the outer surface of RH is attributed to its weak adhesion. Purifying RH from silica may result in better adhesion that may well eliminate the beneficial contribution of silica in the composite. Another way of solving this matter is by integrating a binding agent (Panthapulakkal et al. 2005, Hong et al. 2016, Yang et al. 2005). RH should be dried before processing, as it absorbs moisture that weakened mechanical properties (De Deus et al. 2005).

[*]Instructor, College of Engineering and Geo-Sciences, Caraga State University, Philippines.
[±]Professor, College of Architecture, University of the Philippines, Philippines.

In comparison with inorganic-filler reinforced composite, RH has low CO_2 emission with little to no toxic by-products when burnt, and has reasonable strength and stiffness (Kim et al. 2007, Yang et al. 2006a). As compared to other wood-based materials, RH composite has high resistance to biological attack, excellent termite resistance, and better dimensional stability under moist conditions (Kim et al. 2007).

Polyethylene (PE) and polypropylene (PP) have been the primarily used thermoplastic for processing RH composite (Panthapulakkal et al. 2005, Yang et al. 2004, 2005, 2006a, 2006b, Zhao et al. 2009, Najafi and Khademi-Eslam 2011, Kim et al. 2007, Aminullah et al. 2010, Rosa et al. 2009a). Recently, polyvinyl alcohol (PVA) and polyvinylchloride (PVC) have also been explored in creating RH reinforced composite (Arora et al. 2012).

Integrating binding agents have been studied in manufacturing RH reinforced plastic composite. Maleic anhydride polyethylene (MAPE) on RH/PE composites significantly improves the mechanical and physical properties, with the best properties at 6 wt% (Yang et al. 2005, Chen et al. 2015, Ab Ghani et al. 2014, Ghofrani 2011, Tong et al. 2014). Using maleic anhydride polypropylene as a binding agent improves tensile mechanical and physical properties of the composite, with the best properties at 5 wt% (Yang et al. 2005, Kim et al. 2007, Aminullah et al. 2010, Rosa et al. 2009b, Czél and Kanyok 2007). Scanning electron microscopy (SEM) micrographs indicate that using a binding agent improves interfacial adhesion in the composite (Yang et al. 2005, Aminullah et al. 2010, Rosa et al. 2009b, Ab Ghani et al. 2014, Ghofrani 2011).

On the other hand, fire retardant Borax (BX) and Boric Acid (BA) together denoted in this paper as BX+BA, had been utilized in wood treatment and had been studied in manufacturing fiber-reinforced composite. A study of physical properties shows that the presence of fire retardant BX+BA decreases the water absorption by 50-80% in the urea-formaldehyde sawdust composite (Nagieb et al. 2011). The addition of the binding agent up to 4 wt% improved the water-resistance of the wood plastic composite (Ayrilmis et al. 2012). A BX+BA compound could enhance the decay resistance of wood plastic composite that may be attributed to its high moisture exclusion efficiency (Wu and Xu 2014). The redistribution of BX+BA in commercial cellulosic insulation due to vibration was investigated, and the study shows that the mass loss from cellulosic insulation is negligible when the temperature is below 70 °C at any relative humidity and air exchanges rate from 1.0 to 2.0 volumes per hour (Chiou and Yarbrough 1990).

The study on mechanical properties also exhibits that the increase of fire retardant concentration decreases bending strength in urea-formaldehyde sawdust (Nagieb et al. 2011). Tensile strength and flexural strength also decrease as BX+BA increase in the wood plastic composite (Ayrilmis et al. 2012, Wu and Xu 2014). BA treatment reduced static bending strength, compression strength, and slitting strength perpendicular to grain wood laminated beech veneer lumber (Colakoglu et al. 2003). Studies show that samples with BX provided better mechanical properties compared to those samples with BA in wood-flour plastic composite (Donmez Cavdar et al. 2015). BX had relatively more positive values on impregnation and heat treatment of oak wood (Percin et al. 2015).

Flammability properties of RH plastic composite without fire retardant are closely related to RH loading. Studies show improved flame retardance with the increasing content of RH (Zhao et al. 2009, Bilal et al. 2014). The enhancement was due to the formation of a silica ash layer as a result of the combustion of RH that shields the remaining part of the composite for heat and oxygen leading to slow spread of flame of the composite (Zhao et al. 2009, Arora et al. 2012, Bilal et al. 2014). MAPE, as the binding agent, did not play a significant role in the heat release rate of the composite. Moreover, a slight decrease in values was observed with the increased loading of MAPE (Wu and Xu 2014).

A study using BX+BA shows that the addition of fire retardant decreases the burning rate in a wood plastic composite (Altuntaş et al. 2017). Another paper showed that the reduction of the burning rate was around 50% compared to the control sample on wood flour filled high-density polyethylene composite (Donmez Cavdar et al. 2015). These can be attributed to the wood becoming difficult to ignite, and more oxygen is needed to burn the treated materials, which is consistent with the effect of BX and BA compounds from a protective layer of compact black char (Donmez Cavdar et al. 2015). BA was shown to slow down flame during burning, hindering the attainment of high-temperature values, and also increased the flame collapse time (Karaağaçlıoğlu and Çelik 2012). BA has little effect on flame spread; however, higher char yield is produced in the samples with BA (Donmez Cavdar et al. 2015). BX exhibits better performance for restraining the heat release rate, while BA performs better on smoke suspension and the total amount of heat release. Furthermore, BX+BA aided to reduce the toxic gas production, especially in reducing the insufficient combustion and decreasing the CO production on BX+BA treated bamboo filament (Yu et al. 2017). The best results could be attained with the ideal proportion of (1:1) of BX+BA (Yu et al. 2017, Nagieb et al. 2011).

Thermogravimetric analysis shows that pure plastic sample had a lower initial temperature and higher weight loss speed of thermal decomposition compared to the samples with fire retardant on wood plastic composite (Donmez Cavdar et al. 2015). The addition of BX+BA improves thermal properties at high temperatures and could enhance the formation of char (Wu and Xu 2014).

This experimental research thus aims to develop and test new products of RH reinforced rHDPE composite integrating MAPE as a coupling agent and fire retardant BX+BA, and investigate the effect of different BX+BA treatments on flammability and thermal properties of the composite. Flammability performances of samples were studied according to UL 94 testing, and thermal stability was investigated using the ATSM E1131 "Standard test method for compositional analysis by thermogravimetry."

Experimentation and Testing

Source of Materials

RH was accumulated from a local rice milling plant at Ampayon, Butuan City, Philippines, without further grounding. While emptied bleach plastic bottles

were collected from a local laundry shop at Nasipit, Agusan del Norte, Philippines. Fire retardants BX and BA were obtained from NECO Philippines, Incorporated. MAPE as compatibilizer was obtained from Shanghai Jianqiao Plastic Co., Ltd. in the name of NG1001. The MFI of MAPE was 1.5g/10min, with a density of 0.96 g/cm^3.

Manufacturing Process

Collected RH was oven-dried at 105 °C ± 5 °C for 24 hours to reduce its moisture content and weight (W1) then sealed in a polyethylene bag to ensure its dryness before mixing with fire retardants BX and BA. Collected rHDPE in the form of bleach plastic bottles were cleansed to remove any residual liquid and dirt. Plastic bottles were then cut into small pieces and washed, rinsed, and soaked in warm water for 30 minutes to remove the liquid soap and sun-dried for 8 hours to attain its dryness.

BX and BA were diluted in distilled water at 80 °C, after which the oven-dried RH was submerged and mixed with the concentrations as shown in Table 1. After 24 hours of immersion, excess water was removed, and the impregnated RH with BX/BA was conditioned at room temperature with 60% relative humidity for one week as shown in Figures 1a and 1b. After one week, the impregnated RH/BX/BA was oven-dried at 105 °C ± 5 °C for 24 hours and weighed (W2).

Impregnated RH/BX/BA was mixed with rHDPE and MAPE by a two-roll mill machine with a back-roller temperature of 220 °C and a front roller temperature of 195 °C. First, rHDPE was put into the rolling machine, where it reaches its stage of plasticity. Secondly, MAPE as a binding agent was added. Finally, impregnated RH/BX/BA was gently sprinkled into the rolling plastic as shown in Figures 2a and 2b.

Table 1. *Proposed Formulation of RH Reinforced rHDPE Composite in Weight Percentage*

Sample No.	rHDPE	RH	MAPE	Borax	Boric Acid
1	100	-	-	-	-
2	60	40	-	-	-
3	58.20	38.80	3	-	-
4	57.00	38.00	3	1	1
5	56.40	37.60	3	1.5	1.5
6	55.80	37.20	3	2	2
7	57	38	5	-	-
8	55.80	37.20	5	1	1
9	55.20	36.80	5	1.5	1.5
10	54.60	36.40	5	2	2

Blended rHDPE/MAPE/RH/BX/BA was placed in a 203x203x4 mm thick stainless steel mold and molded by a Shinto compression molding machine with a temperature of 180 °C and a compression strength of 50 kg/cm^2 for 5 minutes. After 5 minutes, the composite was placed in a cool press machine with 50 kg/cm^2

for another 5 minutes and air-cooled before removing the finished product from the mold as shown in Figures 3a and 3b. The composite sample as shown in Figure 4a and 4b, was air-dried for another two days and was cut according to the specific dimension required for material testing.

Figure 1. *Impregnating Process: (a) RH Soaked in Fire Retardant Solution for 24 Hours and (b) Impregnated RH/BX/BA, After Removing Excess Water*

(a) *(b)*

Figure 2. *Reinforcing rHDPE with MAPE and Impregnated RH/BX/BA: (a) Integrating MAPE on Plasticized rHDPE at 200 °C (b) Adding RH/BX/BA on Impregnated rHDPE/MAPE*

(a) *(b)*

Figure 3. *Compression Process: (a) Blended rHDPE/MAPE/RH/BX/BA in 203x203x4 mm Thick Stainless Steel Mold (b) Hot Compression Process of the RH Reinforced rHDPE Composite*

(a) *(b)*

Figure 4. *Finished Product of (a) Pure rHDPE and (b) RH Reinforced rHDPE Composite*

(a) *(b)*

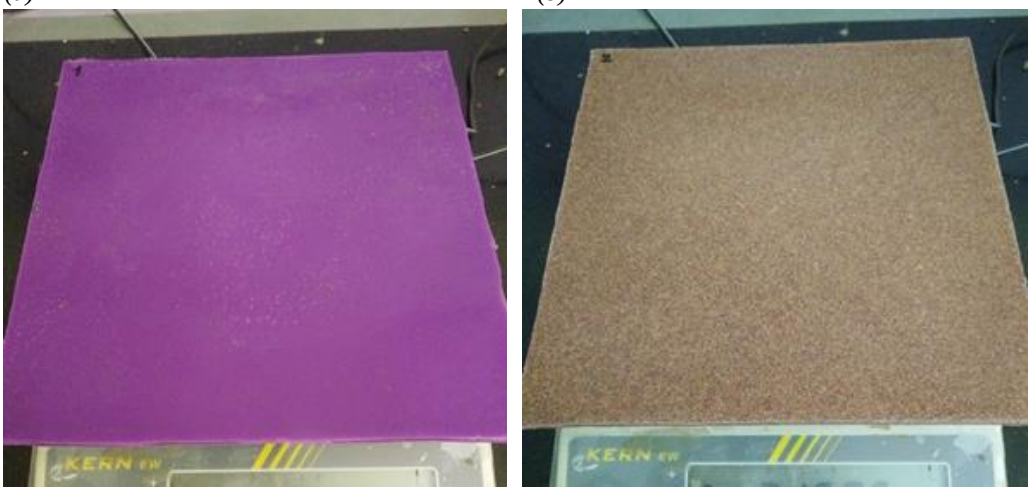

Sample 1 contains 100% of pure rHDPE as the controlled sample. Sample 2 contains RH reinforced rHDPE with 60% rHDPE and 40% RH. Samples 3 and 7 were integrated with MAPE as a binding agent, 3% weight of MAPE for sample 3, and 5% weight of MAPE for sample 7. On the other hand, rHDPE and RH contents were retained at 60% weight of rHDPE and 40% weight of RH, minus the weight percentage of the binding agent MAPE. Samples 4, 5, and 6 were samples with 3% weight of MAPE and 1%, 1.5%, and 2% weight of fire retardant BX and BA,

respectively. rHDPE and RH contents were retained at 60% weight of rHDPE and 40% weight of RH, with the reduction of the weight percentage of MAPE and fire retardant BX and BA. Samples 8, 9, and 10 were samples with 5% weight of MAPE and 1%, 1.5%, and 2% weight of fire retardant BX and BA, respectively. rHDPE and RH contents, on the other hand, were kept at 60% weight of rHDPE and 40% weight of RH, excluding the weight percentage of MAPE and fire retardant BX and BA.

Impregnation of RH with Fire Retardant BX and BA

Oven-dried RH was weighed (W1) and impregnated using a soaking method for 24 hours. Excess water was removed after 24 hours and was conditioned for one week. Subsequently, impregnated RH was oven-dried and weighed (W2) to determine the percentage weight gain (PWG) according to equation

$$PWG\ (\%) = (W2 - W1) \times 100 / W1 \qquad (1)$$

where PWG is the percentage weight gain of the RH after the impregnation process, W1 is the weight of RH before impregnation, and W2 is the weight of RH after the impregnation process (Donmez Cavdar et al. 2015).

UL 94 Testing

The burning rate was investigated by the horizontal burning (HB) test according to UL 94 test standards using Atlas HVUL2 at the Department of Science and Technology, Taguig City, Philippines. Three specimens per sample were cut into 125x13x4mm to be tested. The linear burning rate in millimeters per minute was calculated using the following equation:

$$V = 60\ L/t \qquad (2)$$

where V is the horizontal burning in millimeters per minute from 25 mm to 100 mm benchmark. L is the damaged length in millimeters, and t is time in seconds (UL 94).

The longitudinal axis of the sample is mounted horizontally with its transverse axis at 45 degrees. The flame is applied on the free end for 30 seconds and removed, or as soon as combustion reaches the 25 mm benchmark. Time (t) and length of damage (L) are recorded as combustion travel from 25 mm mark up to 100 mm mark or as soon as it stops. The sample is classified as HB rated if the burning rate does not surpass the 40mm/min or if the fire self-extinguishes before the 100 mm reference point (UL 94).

Thermal Analysis

Thermal analysis of samples was performed according to ATSM E1131 using the TGA Q500 instrument at the Department of Mining, Metallurgical and Materials

Engineering, University of the Philippines. Approximately 35 to 50 mg per sample was tested at a heating rate of 10 °C/min, from 28 °C to 650 °C under an oxygen atmosphere. Weight loss of samples was recorded continuously during the thermal decomposition process (ASTM E1131 – 08).

Results and Discussion

Impregnation Analysis

In Figure 5, it was observed that BX+BA was not entirely infused with RH in terms of weight after the impregnation process, thereby reducing the amount of BX+BA on the actual composition. Data shows that sample number 4 has the highest percentage of absorption among the impregnated samples. Samples number 5 and 9 had the same absorption percentage, while sample number 6 is quite higher by 1% compared to sample number 10. On average, only 43 wt% of fire retardants were absorbed after the impregnation process. Moreover, it has been observed that as fire retardant increases, the percentage of absorption decreases. The loss of weight of BX+BA due to the impregnation process leads to the addition of rDHPE and RH in the actual composition, as shown in Table 2.

Figure 5. *Percentage Weight Gain of RH with BX and BA Before and after Immersion*

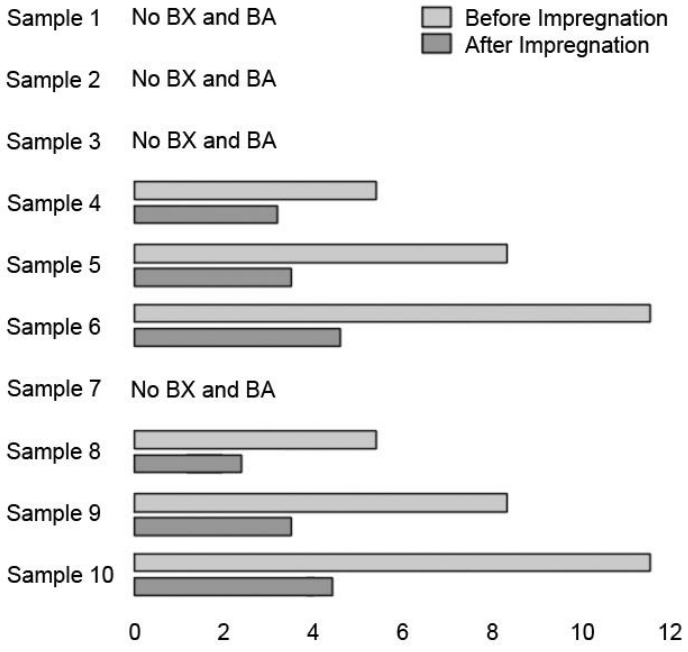

Table 2. *Actual Formulation of RH Reinforced rHDPE Composite in Weight Percentage*

Sample No.	rHDPE	RH	MAPE	Borax	Boric Acid
1	100	-	-	-	-
2	60	40	-	-	-
3	58.20	38.80	3	-	-
4	57.43	38.29	3	0.64	0.64
5	57.38	38.26	3	0.68	0.68
6	57.13	38.09	3	0.89	0.89
7	57	38	5	-	-
8	56.45	37.63	5	0.46	0.46
9	56.21	37.47	5	0.66	0.66
10	55.99	37.33	5	0.84	0.84

Flammability Studies

The results of the UL 94 Horizontal Burning Rate are shown in Figure 6. Data show the average burning rate of specimens per sample. Samples with RH (sample 2) have a 6.03% burning rate reduction compared to the pure rHDPE material (sample 1) that could be attributed to the silica layer created during the combustion of RH that acts as a thermal barrier and heat sink between the fire and the sub-layer of the composite (Bilal et al. 2014). The addition of Maleic Anhydride Grafted Polyethylene as a binding agent to the composite increases the burning rate by about 13% with 3 wt% on sample 3 and 32% with 5 wt% on sample 7 of MAPE compared to rHDPE with RH (sample 2).

Figure 6. *UL 94 Horizontal Burning Rate in Millimeters per Minute*

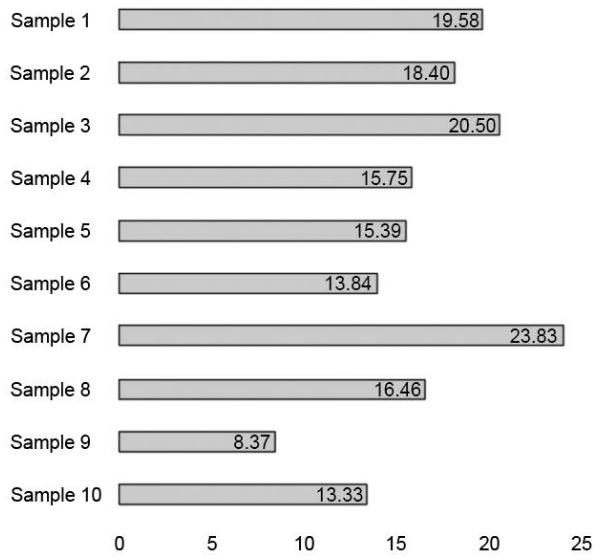

Even though 3 wt% of MAPE increases flammability by 13% compared to RH reinforced rHDPE (sample 2), the addition of BX+BA to the composite enhances flame retardancy by reducing the burning rate of the material. Sample 4

with 1.28 wt% of BX+BA has 23%, sample 5 with 1.36 wt% of BX+BA has 24%, and sample 6 with 1.78 wt% of BX+BA has 32% burning rate reduction.

Incorporating 5 wt% of MAPE increases flammability by 32% compared to RH reinforced rHDPE (sample 2). However, the addition of BX+BA to the composite significantly decreases the flammability by reducing the burning rate of the material. Sample 8 with 0.92% of BX+BA has 30%, sample 9 with 1.32% of BX+BA has 64%, and sample 10 with 1.68% of BX+BA has a 44% burning rate reduction.

Overall, the addition of fire retardant BX+BA to the composite significantly decreases flammability by reducing the burning rate by 26% (samples 4, 5, 6) on average with 3 wt% of MAPE and about 46% (sample 8, 9, 10) on average with 5 wt% of MAPE. The findings further support that the addition of fire retardant BX+BA is an excellent factor for the fire retardancy of the composite (Nagieb et al. 2011, Donmez Cavdar et al. 2015, Yu et al. 2017). MAPE as a binding agent that is known to improve fiber-matrix adhesion between RH and rHDPE and enhanced structural stability of the composite does not show positive enhancement on flame retardancy, as composite displays increased flammability as the amount of binding agent increases. The same was observed on the study of RH polyethylene composite with MAPE as a binding agent (Bilal et al. 2014). However, the addition of the fire retardant BX+BA shows significant improvement on the flammability of the composite even with of the integration of binding agent. These may be attributed to the addition of fire retardant incorporation with the contribution of improving cross-linking between the RH and the fiber-matrix.

Figure 7 exhibits one of three specimens per sample after the horizontal burning test. Noticeably, all nine samples exhibit a char formation except sample 1 of the pure rHDPE sample. Char formation of the nine samples with RH is credited to the silica layer of RH formed during the combustion process. The silica ash shields the composite that hinders the oxygen supply from the heat, leading to a reduction of the spread of flame (Zhao et al. 2009). Furthermore, the addition of BX+BA promotes carbon residue production and fire retardation during the combustion process (Zhao et al. 2009).

Figure 7. *One of Three Specimens per Sample after the UL 94 Horizontal Burning Test*

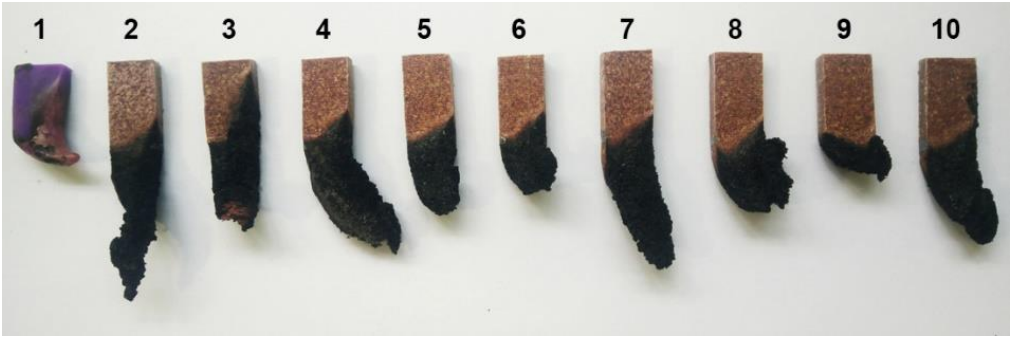

Figures 8a and 8b show the actual horizontal burning test of the materials. Comparatively, pure rHDPE (Figure 8a) exhibits a material degradation as rHDPE

gradually melts as the flame impinges on the specimen, while RH reinforced rHDPE (Figure 8b) displays a stable condition with char formation as it burned.

Figure 8. *Horizontal Burning Test of (a) Pure rHDPE and (b) RH Reinforced rHDPE*

(a) *(b)*

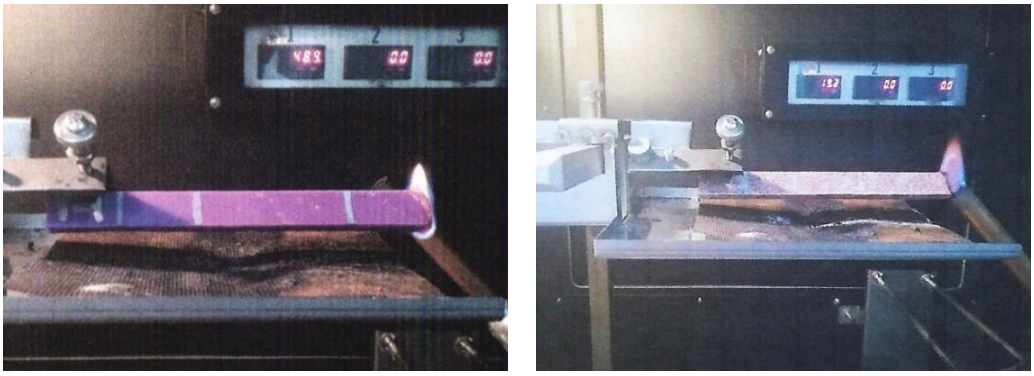

Figures 9a and 9b exhibit the actual horizontal burning test of the materials as the flame reached the 25 mm mark. Relatively, pure rHDPE (Figure 9a) shows a higher flame length corresponding to the highly flammable characteristics of the materials (Whiteley and Pan 1990). On the other hand, RH reinforced rHDPE composite (Figure 9b) presents a favorable condition than pure rHDPE with the evidence of char formation upon burning. The results further support that the flame retardancy mechanism was attributed to thermal protection and the transmission barrier produced by the silica layer created during the burning process (Zhao et al. 2009).

Figure 9. *Horizontal Burning Test at 25 mm Benchmark of (a) Pure rHDPE and (b) RH Reinforced rHDPE*

(a) *(b)*

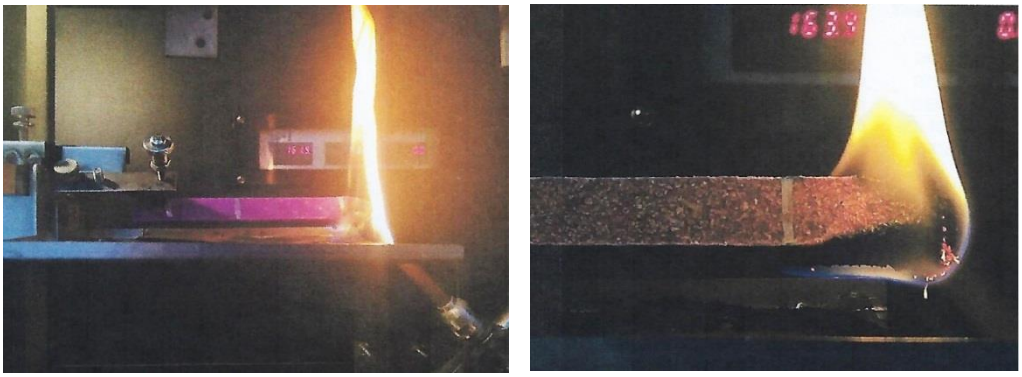

Thermal Studies

Figure 10 represents the thermal degradation of all samples at a heating rate of 10 °C per minute. Unlike rHDPE samples in the related literature (Zhao et al. 2009), sample 1 with pure rHDPE underwent a two-step degradation. The first

weight loss was observed at around 325 °C to 335 °C that loses 70% of its weight, followed by the second degradation process at around 415 °C to 445 °C as the weight reduces to 0.62%. Second stage degradation could be attributed to impurities of the materials, as plastic bottles were cleansed without further purification. It is not manifest what might constitute such behavior; however, a study has reported that foreign materials may be present and the interactions with these impurities of these interactions may exhibit a positive or negative effect on thermal stability (Vásquez-Rendón and Álvarez-Láinez 2018).

Figure 10. *TGA Curves of All Composite Samples at a Heating Rate of 10 °C per Minute under Flowing Oxygen Atmosphere*

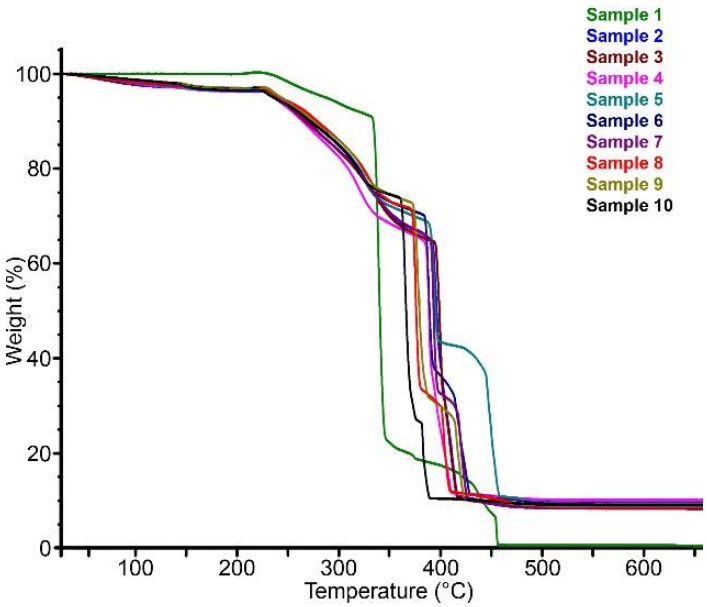

RH reinforced rHDPE (sample 2) underwent a three-stage degradation process; the first stage occurred in the range of 28 °C to 225 °C that measures about 4% weight loss that corresponds to the evaporation of moisture confined on the RH. The second stage of weight reduction happens at 300 °C to 350 °C that corresponds to the decomposition of cellulose and hemicellulose components of RH. The third stage of weight reduction occurs at 380 °C to 410 °C, which corresponds to the decomposition of lignin and rHDPE with 10% weight retention represented by RH ash (Zhao et al. 2009).

Figure 11. *TGA Curves of Pure rHDPE Composite (Sample 1), 60% rHDPE with 40% RH (Sample 2), rHDPE/RH Composite with 3% MAPE (Sample 3) and 5% MAPE (Sample7)*

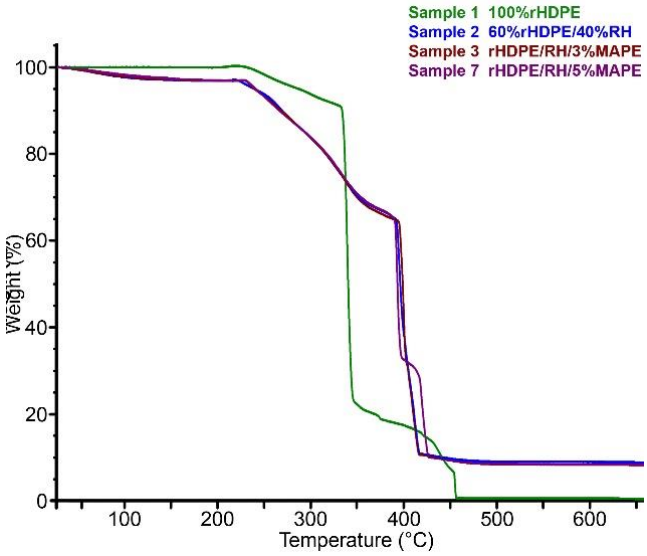

In Figure 11, it is seen that RH reinforced rHDPE composite with 3 wt% of MAPE (sample 3) does not exhibit any significant change in comparison to sample 2 without MAPE. However, increasing the binding agent to 5 wt% of MAPE (sample 7) exhibits another stage of the degradation process. Stage 3 of thermal decomposition happens at 380 °C to 400 °C, and stage 4 degradation follows at 410 °C to 430 °C with 9% weight retention. Thermal stability enhancement on sample 7 could be attributed to interfacial bonding improvement and compatibility between the RH and the matrix due to the treatment of the binding agent.

Figure 12. *TGA Curves of rHDPE/RH with 3%MAPE as a Binding Agent with the Different Fire Retardant Formulations*

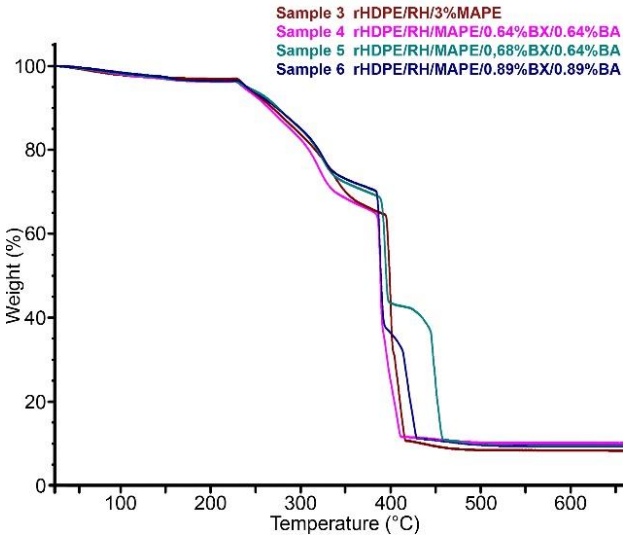

Figure 12 exhibits the TGA of sample 3 (RH composite without fire retardant), sample 4, sample 5, and sample 6 with different concentrations of fire retardant BX and BA with 3 wt% of MAPE. The figure exhibits a similar stage 1 degradation process and slightly different during the second stage of the process. Data also show that the sample with 3 wt% of MAPE without fire retardant (sample 3) is slightly better than sample 4 with 0.64 BX + 0.64 BA. Sample 5 with 0.68 BX + 0.68 BA, on the other hand, shows excellent thermal stability with the new stage of degradation that occurred between 400 °C and 460 °C with 10 wt% weight retention in comparison to sample 6 with 0.89 BX + 0.89 BA with higher fire retardant content. Thermal stability enhancement and the increase of weight retention are credited to the presence of BX that tends to reduce the flame spread (Zhao et al. 2009), and BA elevates the production of carbonaceous char layer resulting in flammability reduction (Intharapat et al. 2016).

Figure 13 shows the thermogravimetric analysis of sample 7 (RH composite without fire retardant), sample 8, sample 9, and sample 10 with different concentrations of fire retardant BX and BA with 5 wt% of MAPE. All samples exhibit a similar stage 1 degradation process, with a variation in stage 2 decomposition process. Data reveals that even though sample 8, sample 9, and sample 10 with fire retardant exhibit an additional stage of thermal degradation, sample 7 with 5 wt% of MAPE without fire retardant agent performs better. The phenomenon could be attributed to interfacial adhesion between RH and rHDPE brought by the integration of MAPE as a binding agent of the composite under fire (Bilal et al. 2014).

Figure 13. *TGA Curves of rHDPE/RH with 5%MAPE as a Binding Agent with the Different Fire Retardant Formulations*

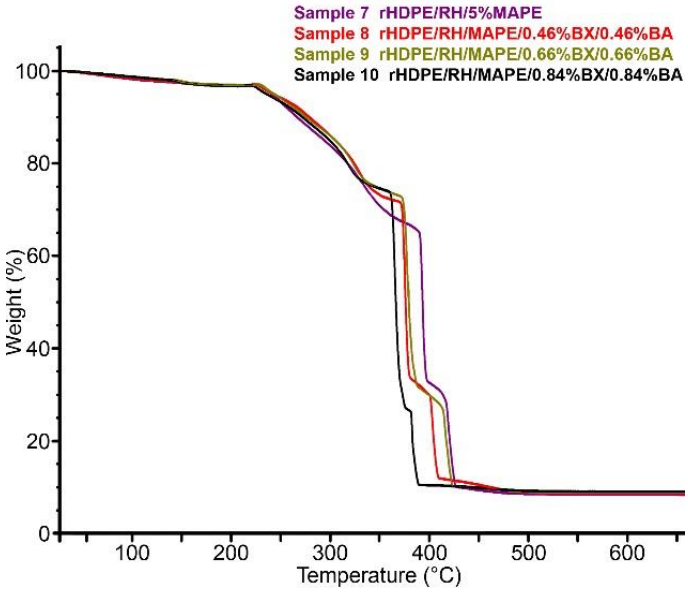

Figure 14. *TGA Curves of Sample 6 (Top), Sample 9 (Bottom Left) and Sample 10 (Bottom Right) in Random Sampling*

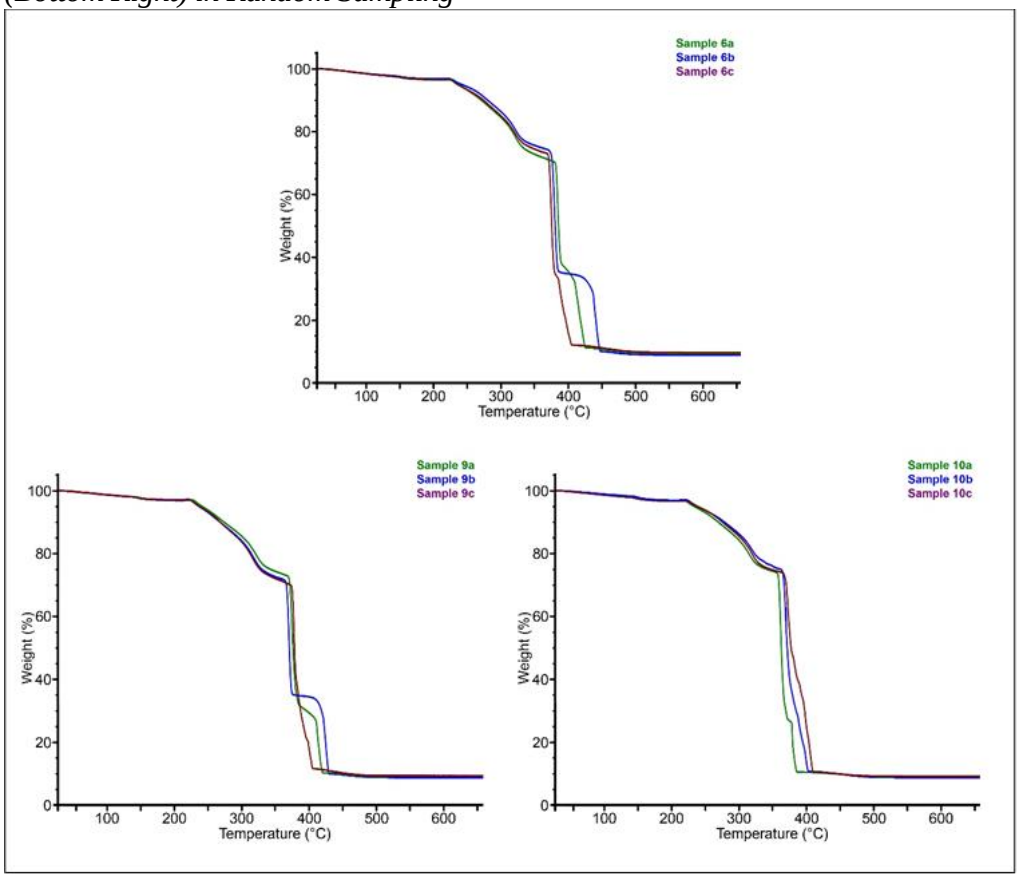

The top 3 samples on flammability were investigated on thermal stability are shown in Figure 14. It was evident that samples 6, 9, and 10 have similar stage 1 degradation with a little deviation on stage 2 as well as stage 3 decomposition. However, a significant variation was clearly exhibited on the stage 4 decomposition process that can be attributed to the integration of MAPE as a binding agent and fire retardant BX and BA. Comparatively, sample 6 with 3 wt% of MAPE as a bending agent performs better with a temperature range of 400 °C to 450 °C than samples 9 and 10 with 5 wt% of the binding agent with 380 °C to 430 °C.

Conclusions

The impregnated RH with fire retardant BX and BA reinforced rHDPE was prepared successfully through twin roll mill and hot compression machine. Based on the UL 94 flammability test and ASTM E1131 thermogravimetry test results of the composite, the following observations were drawn.

On average, the impregnation process enabled the samples to absorb 43 wt% of fire retardant BX and BA. Moreover, the percentage of absorption of the fire retardant decreases as the fire retardant increases.

Flame retardancy of RH reinforced rHDPE was improved in comparison to the pure rHDPE composite. However, the integration of MAPE as a binding agent increases flammability by 13% on 3 wt% and 32% on 5 wt% of MAPE. The addition of fire retardant BX and BA, on the other hand, enhances flame retardancy of the composite, which was clearly observed in the UL 94 horizontal burning test. On average, a reduction of 26% on burning rate with 3 wt%, and 46% with 5 wt% of MAPE. The optimum composition for flammability is at 5 wt% of MAPE with 0.66% BX and 0.66% BA.

The thermal stability of the composite was improved with the addition of RH compared to the pure rHDPE composite. The binding agent, MAPE, did not play a significant role in the thermal stability of the composite at 3 wt%, but slightly improved and exhibited another stage of degradation at 5 wt%. However, the addition of fire retardant BX and BA shows that samples with 3 wt% perform better than samples with 5 wt% of MAPE. Moreover, samples with 5 wt% without fire retardant exhibit better thermal stability than those with a fire retardant agent. Data show that the optimum composition for thermal stability is at 3 wt% of MAPE with 0.68% of BX and 0.68% BA.

Thus, RH performs as an effective ecological fire retardant in the composite, and the addition of BA and BX as non-organic fire retardant that further augment the fire retardancy of the composite makes it favorable in any applications where the fire is an essential parameter with its low flammable properties that will prevent fire hazards in order to protect life and property. We note however that UL 94 is only applicable for devices and appliances. We can explore the possibility of the composite as a candidate for building material like baseboard, moldings, fascia board, ceiling, and wall panel though this may require another testing like UL 263 or ASTM E119 (Kordosky et al. 2020, Amat et al. 2012).

References

Ab Ghani MH, Salleh MN, Chen RS, Ahmad S (2014) The effects of rice husk content on mechanical and morphological properties of recycled polymer biocomposites. *American-Eurasian Journal of Sustainable Agriculture* 8(4): 128–134.

Altuntaş E, Karaoğul E, Alma MH (2017) Effect of boron compounds on the thermal and combustion properties of wood-plastic composites. *Turkish Journal of Forestry* 18(3): 247–250.

Amat RC, Ibrahim NM, Rahim NL, Tajudin NSBA, Ahmad KR (2014) Fire resistance of biomass ash panels used for internal partitions in buildings. *Procedia Engineering* 53(Jan): 52–57.

Aminullah A, Syed Mustafa SJ, Nor Azlan MR, Mohd Hafizi N, Mohd Asri I, Rozman HD (2010) Effect of filler composition and incorporation of additives on the mechanical properties of polypropylene composites with high loading lignocellulosic materials. *Journal of Reinforced Plastics and Composites* 29(20): 3115–3124.

Arora S, Kumar M, Kumar M (2012) Flammability and thermal degradation studies of PVA/rice husk composites. *Journal of Reinforced Plastic Composites* 31(2): 85–93.

ASTM E1131 − 08. *Standard test method for compositional analysis by thermogravimetry 1*. ASTM International 2015: 6.

Ayrilmis N, Akbulut T, Dundar T, White RH, Mengeloglu F, Buyuksari U, et al. Effect of boron and phosphate compounds on physical, mechanical, and fire properties of wood-polypropylene composites. *Construction and Building Materials* 33(Aug): 63–69.

Bilal A, Lin RJT, Jayaraman K (2014) Optimisation of material compositions for flammability characteristics in rice husk/polyethylene composites. *Journal of Reinforced Plastics and Composites* 33(22): 2021–2033.

Chand N, Sharma P, Fahim M (2010) Tribology of maleic anhydride modified rice-husk filled polyvinylchloride. *Wear* 269(11-12): 847–853.

Chen RS, Ab Ghani MH, Ahmad S, Salleh MN, Tarawneh MA (2015) Rice husk flour biocomposites based on recycled high-density polyethylene/polyethylene terephthalate blend: effect of high filler loading on physical, mechanical and thermal properties. *Journal of Composite Materials* 49(10): 1241–1253.

Chiou N, Yarbrough DW (1990) Permanency of boric acid used as a fire retardant in cellulosic insulation. *Energy and Buildings* 14(4): 351–361.

Colakoglu G, Colak S, Aydin I, Yildiz UC, Yildiz S (2003) Effect of boric acid treatment on mechanical properties of laminated beech veneer lumber. *Silva Fennica* 37(4): 505–510.

Czél G, Kanyok Z (2007) MAgPP as an effective coupling agent in rice husk flour filled polypropylene composites. *Materials Science Forum* 537(Feb): 137–144.

De Deus JF, Monteiro SN, D'Almeida JRM (2005) Effect of drying, molding pressure, and strain rate on the flexural mechanical behavior of piassava (Attalea funifera Mart) fiber-polyester composites. *Polymer Testing* 24(6): 750–755.

Donmez Cavdar A, Mengeloɔlu F, Karakus K (2015) Effect of boric acid and borax on mechanical, fire and thermal properties of wood flour filled high density polyethylene composites. *Measurement* 60(Jan): 6–12.

Ghofrani M (2011) A study on rice-husk/recycled high density polyethylene composites - their physical and mechanical properties. *Environmental Sciences* 9(1): 99–112.

Hong H, Li X, Liu H, Zhang H, He H, Xu H, et al. (2016) Transform rice husk and recycled polyethylene into high performance composites: using a novel compatibilizer to infiltratively enhance the interfacial interactions. *Progress in Rubber, Plastics and Recycling Technology* 32(4): 253–268.

Intharapat P, Nakason C, Kongnoo A (2016) Preparation of boric acid supported natural rubber as a reactive flame retardant and its properties. *Polymer Degradation and Stability* 128(Jun): 217–227.

Karaağaçlıoğlu İE, Çelik MS (2012) Effect of boric acid on fire retardant properties of compressed mineral added cellulosic insulators. In Proceedings of the *XIIIth International Mineral Processing Symposium*, 1–8. Bodrum, Turkey.

Kim HS, Lee BH, Choi SW, Kim S, Kim HJ (2007) The effect of types of maleic anhydride-grafted polypropylene (MAPP) on the interfacial adhesion properties of bio-flour-filled polypropylene composites. *Composites Part A: Applied Science and Manufacturing* 38(6): 1473–1482.

Kordosky AN, Drury MM, Quiel SE (2020) Structural fire resistance of partially restrained, partially composite floor beams, I: experiments. *Journal of Constructional Steel Research* 167(Apr): 105945.

Nagieb ZA, Nassar MA, El-Meligy MG (2011) Effect of addition of boric acid and borax on fire-retardant and mechanical properties of urea formaldehyde saw dust composites. *International Journal of Carbohydrate Chemistry* (Nov): 1–6.

Najafi A, Khademi-Eslam H (2011) Lignocellulosic filler/recycled HDPE composites: effect of filler type on physical and flexural properties. *BioResources* 6(3): 2411–2424.

Panthapulakkal S, Law S, Sain M (2005) Enhancement of processability of rice husk filled high-density polyethylene composite profiles. *Journal of Thermoplastic Composite Materials* 18(5): 445–458.

Percin O, Sofuoglu SD, Uzun O (2015) Effects of boron impregnation and heat treatment on some mechanical properties of oak (Quercus petraea Liebl.) wood. *BioResources* 10(3): 3963–3978.

Rosa SML, Nachtigall SMB, Ferreira CA (2009a) Thermal and dynamic-mechanical characterization of rice-husk filled polypropylene composites. *Macromolecular Research* 17(1): 8–13.

Rosa SML, Santos EF, Ferreira CA, Nachtigalt SMB (2009b) Studies on the properties of rice-husk-filled-PP composites - Effect of maleated PP. *Materials Research* 12(3): 333–338.

UL 94. *Tests for flammability of plastic materials for parts in devices and appliances*. 2013. Available at: https://standardscatalog.ul.com/standards/en/standard_94_6.

Vásquez-Rendón M, Álvarez-Láinez ML (2018) Tailoring the mechanical, thermal, and fl ammability properties of high- performance PEI / PBT blends exhibiting dual-phase continuity. *Polymer* 154(76): 241–252.

Whiteley MJ, Pan WP (1990) A study of the flammability of chlorinated polyethylene under pyrolysis conditions. *Thermochimica Acta* 166(Sep): 27–39.

Wu GF, Xu M (2014) Effects of boron compounds on the mechanical and fire properties of wood-chitosan and high-density polyethylene composites. *BioResources* 9(3): 4173–4193.

Yang HS, Kim HJ, Son J, Park HJ, Lee BJ, Hwang TS (2004) Rice-husk flour filled polypropylene composites; mechanical and morphological study. *Composite Structures* 63(3-4): 305–312.

Yang HS, Kim HJ, Park HJ, Lee BJ, Hwang TS (2005) Effect of compatibilizing agents on rice-husk flour reinforced polypropylene composites. *Composite Structures* 77(1): 45–55.

Yang HS, Kim HJ, Park HJ, Lee BJ, Hwang TS (2006a) Water absorption behavior and mechanical properties of lignocellulosic filler-polyolefin bio-composites. *Composite Structures* 72(4): 429–437.

Yang HS, Wolcott MP, Kim HS, Kim S, Kim HJ (2006b) Properties of lignocellulosic material filled polypropylene bio-composites made with different manufacturing processes. *Polymer Testing* 25(5): 668–676.

Yu L, Cai J, Li H, Lu F, Qin D, Fei B (2017) Effects of boric acid and/or borax treatments on the fire resistance of bamboo filament. *BioResources* 12(3): 5296–5307.

Zhao Q, Zhang B, Quan H, Yam RCM, Yuen RKK, Li RKY (2009) Flame retardancy of rice husk-filled high-density polyethylene ecocomposites. *Composites Science and Technology* 69(15-16): 2675–2681.

Athens Journal of Technology and Engineering - Volume 9, Issue 1, March 2022 – Pages 61-76

Discrete-Events Simulation for Teaching Statistics in Industrial Engineering

By Farida Saïd[*], Iehann Eveno[±] & Jeanne Villaneau[°]

This paper presents a discrete events simulation tool developed to support undergraduate students in their Statistics and Data Analysis course. Although the use of modern smart technologies in the industry contributes to a profusion of data, very few enterprise datasets are freely available, resulting in a serious lack of open real-world data for research and education. To overcome this difficulty, we designed a tool that simulates scheduling scenarios in a manufacturing environment. The generated data may be used to put statistical concepts and methods into practice to design cost-effective strategies for optimizing key performance indicators, such as reducing production time, improving quality, eliminating wastes, and maximizing profits.

Keywords: *industrial datasets, teaching statistics, discrete events simulation*

Introduction

Industrial engineering (IE) is the branch of engineering that deals with improving processes, systems, or organizations and designing goods or services in the most efficient way possible, saving money, time, raw resources, labor, and energy while complying with safety standards and regulations. Industrial engineers use scientific and technical knowledge and skills to integrate and operate complex systems, and as such, their training programs have a significant scientific component. IE educators appear to agree on IE knowledge and curriculum structure while continually seeking innovations in content and instruction (Lang et al. 1999, Davies 2001, Carrera 2006, Eskandari et al. 2015, Lima et al. 2012, Sackey and Bester 2016). In comparative studies, there is consensus that statistics and data analysis are part of the core courses in IE programs, and contextualizing learnings by working with realistic data is highly recommended to help students better understand their future profession (Kuo 2001, Fraser and Teran 2006, Nguyen and Nguyen 2018).

Five main features of authentic contexts have been proposed (Cobb 1999, Fosnot 1996, Tynjala 1999), and they provide a theoretical justification for the inclusion of realistic contexts in teaching and assessment processes (Libman 2010): 1) *practical significance*: Lave and Wegner (1991) argue that knowledge is situated and contextual and, therefore, the material studied must be related to real situations in which students are likely to use it; 2) *complexity and challenge*: in real life, events always present a wealth of data and conditions that can be studied

[*]Associate Professor, University of South Brittany, France.
[±]R&D Engineer, University of South Brittany, France.
[°]Emeritus Associate Professor, University of South Brittany, France.

from different angles and approached from multiple perspectives. Mirroring this, a learning situation that encourages personal investigation in a realistic context is rich and complex; it does not prescribe a single correct way of learning about reality or a single correct answer (Kirschner et al. 2006). Students are challenged and respond by formulating their own questions, developing their own models and explanations, and examining their own results (Garfield and Ben-Zvi 2007); 3) *relevance and motivation*: relevance refers to the fact that if the context is meaningful enough for the learner to appropriate it, then she or he can harness her or his energy to invest what is necessary to acquire a deep understanding of the subject matter and readiness to use it (Driver et al. 1994); 4) *interconnectedness and transfer*: this argument concerns the importance of authentic context in using the learned material to solve new problems and empower the learner. With real-life data, students learn significantly more about how to figure out an appropriate combination of rules for each new problem and how to use it for problem-solving (Gergen 1995, Hmelo-Silver 2004); 5) l*earner empowerment*: teaching and assessment processes that encourage personal investigation in a realistic context enhance the role of the learner (Eisner 1999, Graves 2002). Because students know the situation they are studying, they become somewhat experts and can take the initiative, raise questions and issues, and bring up topics for discussion with the teacher or their peers. In this way, they acquire knowledge that can go beyond the topic under investigation.

Consistent with these considerations, a large body of research has been conducted to improve the educational experience of statistics students, and they agree on the added value of using real-world data (Willett and Singer 1992, Scheaffer 2001, Bryce 2005, Russell et al. 2011). There is general agreement that statistics are taught more effectively using real-world data (Cobb and Moore 1997), and some research suggests that students consider the use of real-world datasets to be relevant to learning, interesting, motivating, promoting greater involvement and engagement, and lending itself to greater understanding (Neumann et al. 2013). In addition, the use of real-world datasets gives the learning experience a more personal character that increases interest in learning (Chottiner 1991). However, presenting applied problems in a course does not automatically increase motivation; what is essential is how students work with real-life data. According to (Biggs and Tang 2011), students are motivated if they perceive their task as reasonable and beneficial in some way. They should find the task useful for understanding the theory, for the exam, or for their future professional life. In addition, data collection by students themselves has an increased benefit to learning (Hogg 1991).

In their search for realistic contexts, instructors generally use actual real-life data, simulated data, or data derived from real-life datasets by simulation (Luse and Burkman 2018). A major problem with real-world data is that it is not freely available for teaching and research. For example, in the IE field, we could take advantage of the large amounts of data produced by companies driven by digital transformation and the increasing use of connected devices and interconnected machines. However, as this data is at the heart of manufacturing systems, it is rarely shared or freely available, resulting in a serious lack of real open data for

research and education. Various simulation tools have been developed to overcome this difficulty, some of which are free[1], to generate data that has the complexity and nuances of actual real-world data.

To support IE undergraduate students at the University of South Brittany (France) in their one-semester course on statistics and data analysis, we developed a simulation tool in the agri-food domain. It simulates the operation of a pastry factory based on discrete-events simulations (DES) (Elizandro and Taha 2007). Simulation models are usually built to understand how systems behave over time and compare their performance under different conditions. DES models are widely used for design and implementation tasks, operational analysis, advanced planning, resource allocation, and logistics management. They are also commonly used for scheduling and automation, at the heart of Industry 4.0 (Ram and Davim 2018).

The main objective of our simulation tool is to create realistic industrial experiments and data to put into practice data analysis methods (sampling, confidence intervals, hypothesis testing, regression models). Our tool considers the parameters and data formats that students encounter most in their professional lives. The input parameters of the simulator are typical of the ERP (Enterprise resource planning) data, and the outputs are typical of the SCADA (Supervisory control and data acquisition) feedback. The simulated data can be used, among others, to (1) identify the most significant key performance indicators (overall equipment effectiveness, capacity…) through the analysis of production behavior; (2) determine critical phases of the production process and understand the involvement of the physical environment in the quality of production.

We use this tool to practice the concepts studied in the Statistics and Data Analysis course, namely descriptive statistics, confidence intervals, hypothesis testing, and linear and logistic regression models. Following the approach studied by (Gratchev and Jeng 2018) and applied by (Carr M, Fhloinn 2016, Farell and Carr 2019), we use a "hybrid" pedagogical approach. We present the basic concepts in statistics and probability in the traditional approach in class, and then a project is introduced to consolidate the theory covered while allowing students to apply it in realistic situations. For the project, students work in small groups of 2 or 3 on datasets generated by the simulation tool, one per group. Students must formulate practical questions that they answer using the statistical methods studied. Real-world statistical projects aim to improve students' understanding of the material and help them develop their problem-solving, teamwork, and oral and written communication skills.

The paper is organized as follows: in the next section, we describe the simulated manufacturing system, followed by a section on how we designed the simulation tool and the experiments it allows. In the "Results Analysis Framework" section, we present an experiment, some simulated results, and their use in the student project. We conclude with a discussion and some perspectives.

[1]https://en.wikipedia.org/wiki/List_of_discrete_event_simulation_software.

The Manufacturing System

The manufacturing system in focus includes the four main activities shown in Figure 1. Various raw materials (eggs, butter, sugar, flour) are mixed and kneaded to form a dough shaped into pastries and baked in batches in an oven. Once cooked, the pastries are packed and palletized. Quality control takes place after the bagging phase; it consists in testing a random sample of pastries from a lot and deciding whether to accept or reject the whole lot based on the quality of the random sample.

Figure 1. *Main Activities of the Manufacturing Process*

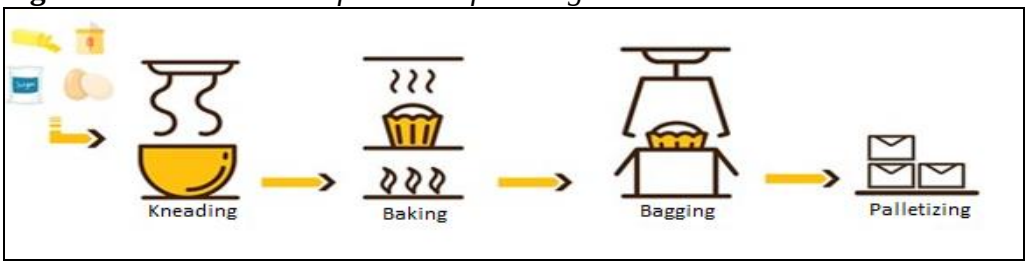

There are many factors involved in performing the activities, and a disruption in any one of them affects the rest of the process. For example, a stopping during baking results in under-baked or over-baked pastries and their subsequent disposal, which, in turn, affects the number of packaged, palletized, and sold products.

According to Schruben and Schruben (2001), the rules or factors that govern the interaction of entities in a system are called parameters if they cannot be controlled and laws if they are controllable. Figure 2 shows some of the parameters and laws of our manufacturing system; one can refer to Table 1 for a list of the main factors.

Figure 2. *Manufacturing System*

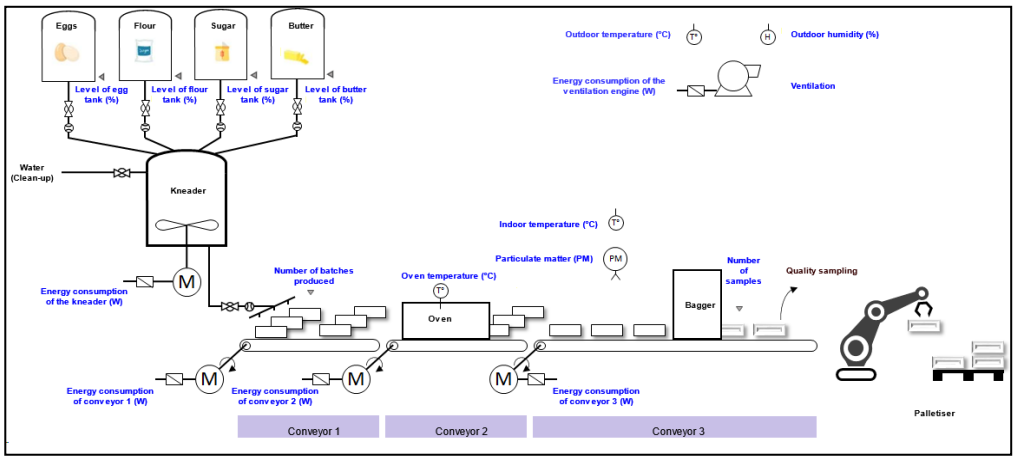

Table 1. *Main Manufacturing System Factors*

Equipment shutdown by equipment (0, 1)
Equipment failure by equipment (0, 1)
Oven temperature (°C)
Amount of each ingredient needed to make a lot of pastries (% of the tank size)
Number of rejects during a run
Level of each ingredient tank during production (%)
Maximal level of each ingredient tank
Maximal refill time for each ingredient tank (seconds)
Minimal refill time for each ingredient tank (seconds)
Refill time for each ingredient tank during production (seconds)
Maximal number of staffers
Minimal number of staffers
The actual number of staffers
Time spent in the oven (min)
Time spent on the conveyor 3 (min)
Quality of the sampled items
Disposal thresholds
Random disposal thresholds

The Simulation Tool

A manufacturing system is a combination of resources (machines, people, raw materials...), planning, organizational structures, information flows, and IT-systems that aim to achieve the manufacture of an economic product cost-effectively. To understand how systems behave over time and to compare their performance under different conditions, two types of simulation models can be built: (1) discrete-event dynamic system models where the operation of the system is represented as a chronological sequence of events, and (2) continuous-event dynamic systems that track systems responses over time according to a set of equations involving usually differential equations.

We adopted the discrete-event simulation (DES) approach which is generally used to model workflow as a network of queues and activities where state changes occur at discrete and irregular time stamps. DES models are generally stochastic, and randomness is generated using statistical distributions.

The general framework of the simulation is depicted in Figure 3. It proceeds in the following steps for a single run: (1) the user selects a combination of input factors related to the manufacturing system, the environment, and the simulation. (2) depending on the stated inputs, a variety of failures can be generated. These can be random or functional (they follow statistical distributions). In case of failure, an intervention request is launched. It feeds a knowledge base of failures and repair response times according to the type of failure, the number of available staffers, and the failure time occurrence (hour, day, month). (3) The laws of the industrial process are adapted to the inputs and, (4) the production process is launched. (5) An assurance sampling is carried out; it consists of selecting some

items in a lot and deciding whether to accept or reject the entire lot based on the inspection of the sample. (6) The output data are stored in a spreadsheet (CSV file) for subsequent statistical analysis: one line per run. (7) the simulation tool updates the input settings for a new run.

Figure 3. *Simulation Framework*

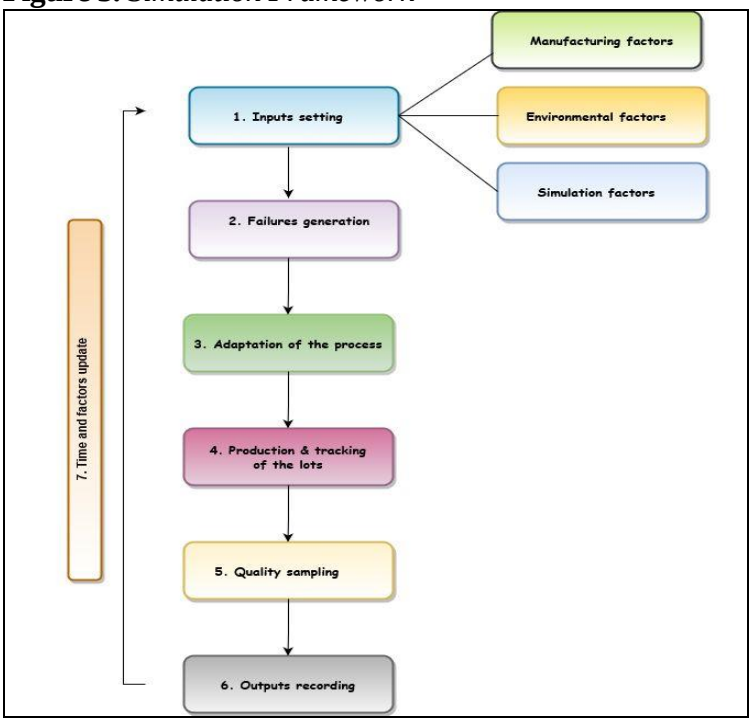

The factory's operation can be simulated over long periods - up to one year - with a time increment of one minute at least. Table 2 describes the main factors involved in the simulation process at different stages.

The simulation outputs are provided in Table 3. Among them is the production quality indicator which is calculated as a linear combination of 5 stochastic quality indicators: 1) a baking quality indicator which corresponds to the time spent by a batch of pastries in the oven. It follows a Gaussian distribution around a theoretical baking time with a given standard deviation; 2) an error function that ensures that products that have been in the oven for a long time are not systematically rejected if the oven is at low temperature; 3) a Humidex[2] index which combines temperature and humidity in one computed value. The higher the Humidex, the softer the cakes and the more mold can develop. Conversely, if the Humidex is too low, the cakes are too dry and therefore of poor quality; 4) a ppm quality indicator which corresponds to an error function that reflects the quantity of particles suspended in air; 5) a cooling quality indicator which corresponds to an error function that reflects the time spent by a batch of pastries between the oven and the bagger; this is a critical time during which bacteria can grow. Production quality is

[2]https://en.wikipedia.org/wiki/Humidex.

a standardized metric with values ranging from 0 to 1. The closer the value is to 1, the higher is the production quality.

The simulation tool was implemented in Python 3.6 with standard libraries.

Table 2. *Main Simulation Factors*

Time	Start date of the simulation: parameter
	Simulation during weekends (yes, no)
	No simulation on Friday afternoons for clean-up (yes, no)
Failure generation	Failure simulation (yes, no)
	Time occurrence
	Number of runs before failure per equipment
	Repair response time per equipment
	Range of the response time per equipment
	Range of the random failures per equipment
Sampling	Sampling range per hour of operation
Outputs	Recording of the data (yes, no)
	Recording increment (day, minute)
Environment	Indoor and outdoor temperatures (°C)
	Outdoor humidity (%)
	Particulate matter (ppm)
	Range of particulate matter when the fan is on (ppm)
	Thresholds that set the increase and decrease of the indoor temperature (°C)
Production	Theoretical time to produce a lot (seconds)
	Number of pastries in a lot
	Weight of a pastry (g)
	Number of lots produced during a run
	Theoretical power consumption per engine equipment (W)
	Thresholds for PID and engine power consumption (W)
	Refill time for raw material tanks (min)
	Temperature thresholds for fan operation (°C)
	Thresholds for increase and decrease of indoor temperature and particulate matter
	Thresholds for baking quality indicators, humidity index, ppm quality indicator, cooling quality indicator

Table 3. *Output Variables*

Categorical variables	Continuous variables	Discrete variables
Day and Daytime	Weekly production load: %	Number of staffers
Equipment Failure (oven, kneader, bagger, fan, conveyors): yes, no	Equipment downtime (oven, kneader, bagger, fan, conveyors): min	Number of lots produced
	Energy consumption per equipment (oven, kneader, bagger, fan, conveyors): W	Number of samples
	Production quality indicator	Number of rejects
	Tank level per ingredient (egg, flour, butter, sugar): %	
	Outdoor temperature: °C	
	Indoor temperature: °C	
	Outdoor humidity: %	
	Oven temperature: °C	
	Particulate matter: ppm	

Output Analysis Framework

After designing a simulation model and implementing a corresponding program, appropriate output analyses must be performed. As shown in Figure 4, the main activities related to analyzing output data are experimentation, drawing reliable conclusions, communication, and presentation.

Figure 4. *Output Analysis Framework*

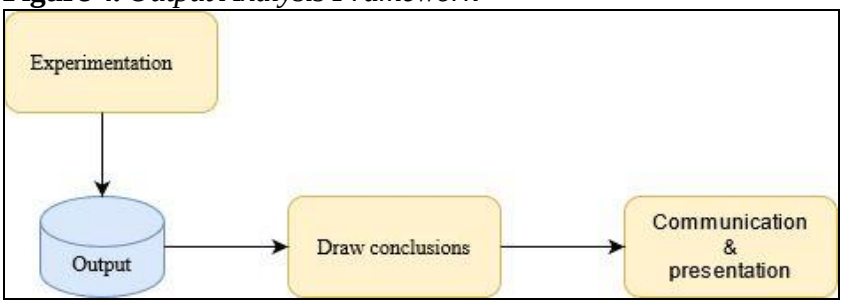

When setting up the simulation experiment, it is necessary to choose the type of simulation to perform. There are generally two types of simulations: terminating and non-terminating. The difference between them is whether one is interested in the system's behavior over a given period (final production counts, time-changing behavior) or in the steady-state behavior of the system (overall average behavior). Experiments involving terminating simulations are typically conducted by running multiple simulations, or replications, of the period of interest using a different random seed for each run. This procedure allows for statistically independent and unbiased observations of the system response over the simulated period. The three questions that need to be answered when running a terminating experiment are: what the model's initial state should be, the terminating event or time, and how many replications to do.

The problems associated with producing meaningful output statistics for terminating simulations are different from those for non-terminating systems. In steady-state simulations, we face the following problems: determining the initial warm-up period, choosing among several alternative methods for obtaining sample observations, and determining the run duration.

In the context of our course, we were interested in terminating simulations.

Cases of Study

We simulated ten months of operation of the factory, from 1 March to 31 December. The weekly production load during the simulated period is given in Figure 5. For example, from 1 March to 21 March inclusive, the production load per week was 70%.

Figure 5. *Weekly Production Load (%)*

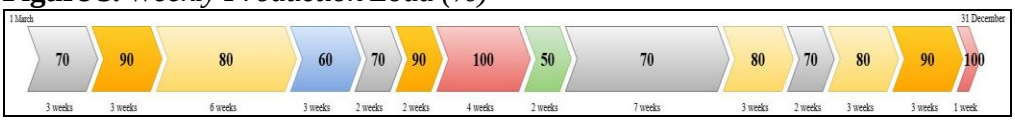

Quality sampling was carried out every two hours, starting at 00:00 for 13 minutes. In the following, we introduce the categorical variable Daytime which refers to the sampling periods (cf. Table 4).

Table 4. *Categorical Variable Daytime*

Sampling period	00:00 00:13	02:00 02:13	04:00 04:13	06:00 06:13	08:00 08:13	10:00 10:13
Daytime	0am	2am	4am	6am	8am	10am
Sampling period	12:00 12:13	14:00 14:13	16:00 16:13	18:00 18:13	20:00 20:13	22:00 22:13
Daytime	12am	2pm	4pm	6pm	8pm	10pm

We recorded 3762 entries, one per sample, and for each sample, the variables in Table 4 were filled in.

In what follows, we answer two questions raised by the students regarding the simulated data using some of the methods studied in the Statistics and Data Analysis course. All analyses were performed in R, a free data analysis software (R Core Team 2021). Assumptions' validity is always checked prior to performing the tests; however, we present them after the results for convenience.

> Question 1: What is the impact of fan failures on the factory's indoor temperature and particulate matter?

Temperature

We used a two-sided independent t-test to determine if there is a statistical difference between the average indoor temperatures in case of fan failure (N_1=2148, m_1=21.73, s_1=1.93) versus no fan failure (N_2=1524, m_2=18.32, s_2=1.83). We found out that fan failures significantly increase the indoor temperature of the factory ($t(3670)$=53.95, p<0.001). Cohen's d (1.81) suggests that this is a large effect. The 95% confidence interval (CI) for the difference between temperature means is 3.29°C - 3.54°C and it suggests that the true increase in temperature means is likely to be within this range 95% of the time. Figure 6 depicts the 95% CIs of the indoor temperature by fan failure occurrence; the centers of the CIs are connected by segments for better graphical readability.

The assumptions of the independent t-test require: (1) independence of the two groups (with and without fan failures groups are independent); (2) the dependent variable should be approximately normally distributed in each group. The QQ-plots in Figure 7 show deviation from normality of the two distributions, which is confirmed by Shapiro-Wilk tests (without fan failures: W_1=0.93, p<0.001; with fan failures: W_2=0.92, p<0.001). However, we have very large sample sizes, and we can still use t-tests; (3) homogeneity of variance is tested using Levene's

test of comparison of variances and it showed no difference between the variances of the two groups.

Figure 6. *95% CIs for Indoor Temperature*

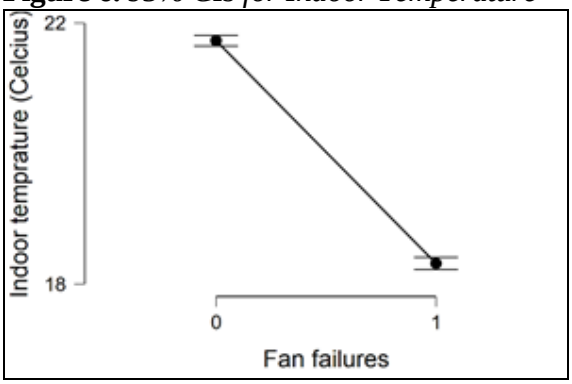

Note: 0 and 1 stand for "without" and "with" fan failures respectively.

Figure 7. *QQ-Plots of Indoor Temperature*

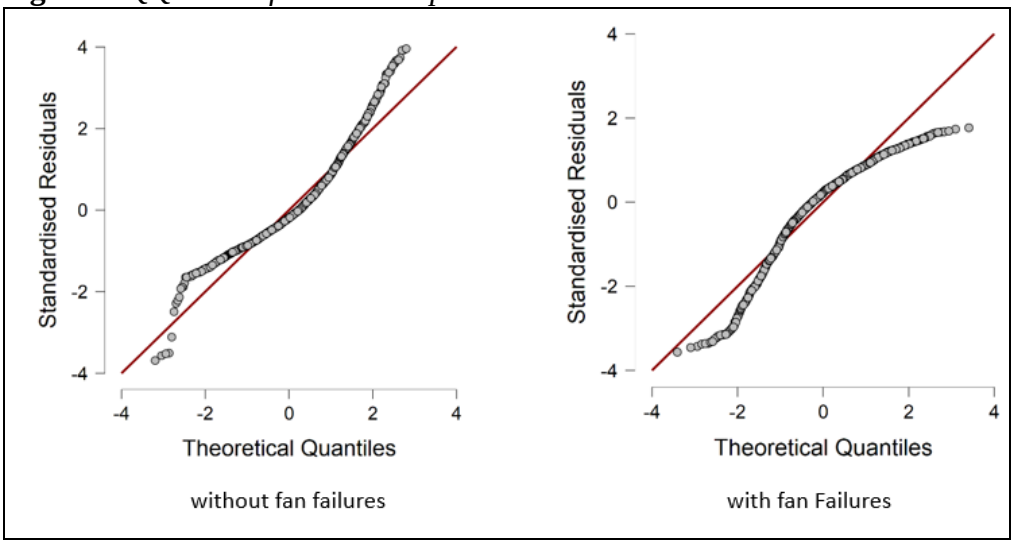

Particulate Matter

We used a two-sided independent Welch's t-test to compare the average indoor temperatures in case of fan failure (N_1=2148, m_1=611.36, s_1=181.99) versus no fan failure (N_2=1524, m_2=607.63, s_2=154.19). There is no evidence of an effect of fan failures on the amount of particulate matter in the air (t(3556.7)=0.67, p=0.50 ns); Figure 8 shows the large overlap of the 95% confidence intervals of the two groups.

Shapiro-Wilk tests showed a normality violation of indoor temperature in each of the two groups (without fan failure: W_1=0.91, p<0.001; with fan failure: W_2=0.97, p<0.001). In addition, Levene's test showed a significant difference between variances. We accounted for these violations using the adjusted Welch's t-test statistic, which is robust for skewed distributions and large sample sizes.

Figure 8. *95% CIs for Particulate Matter*

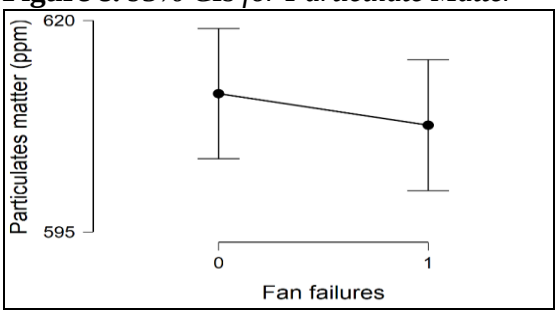

Note: 0 and 1 stand for "without" and "with" fan failures respectively.

Question 2: Does the production quality indicator change over time and is it affected by the weekly charge load?

Tables 5 and 6 provide descriptive statistics of the production quality indicator by weekly charge load and daytime respectively. Differences in average quality scores can already be observed by weekly load and over time. It is yet to investigate whether these differences are significant and whether there is an interaction effect between the weekly production load and the sampling timetable.

Table 5. *Production Quality Indicator by Weekly Production Load*

	Weekly charge load (%)					
	50	60	70	80	90	100
Sample size	504	252	839	1008	672	393
Mean	0.87	0.77	0.89	0.85	0.85	0.78
Std. Deviation	0.07	0.05	0.08	0.09	0.09	0.07
Minimum	0.63	0.57	0.60	0.57	0.53	0.60
Maximum	0.98	0.91	0.98	0.98	0.97	0.96

Table 6. *Production Quality Indicator over Time*

	Daytime											
	0am	2am	4am	6am	8am	10am	12am	2pm	4pm	6pm	8pm	10pm
Sample size	305	306	306	306	306	306	306	306	305	305	305	306
Mean	0.86	0.86	0.84	0.85	0.87	0.86	0.84	0.84	0.87	0.86	0.83	0.84
Std. Deviation	0.09	0.09	0.09	0.09	0.09	0.09	0.09	0.09	0.09	0.09	0.09	0.09
Minimum	0.63	0.63	0.60	0.64	0.60	0.61	0.61	0.57	0.60	0.57	0.63	0.53
Maximum	0.98	0.97	0.96	0.97	0.98	0.97	0.96	0.97	0.98	0.98	0.96	0.96

A two-way independent Anova (Analysis of variance) was conducted to examine the effect of the weekly production load and daytime on the production quality indicator. There were significant main effects for both weekly production load ($F(5,3595)$=147.62, p<0.001) and daytime ($F(5,3595)$=6.51, p<0.001). There was no evidence of an interaction effect ($F(55,3595)$=0.26, ns). Omega squared measure suggests a large main effect of the weekly production load (ω^2=0.17) and a small effect of daytime (ω^2=0.014). After checking Anova's assumptions, we carry out post hoc testing to go further.

Effect of the Weekly Production Load

Figure 9 depicts the behavior of the production quality according to the weekly production load; p-values and confidence intervals are adjusted for comparing a family of 6 estimates using Tukey's correction method. The centers of the confidence intervals are connected by segments for better graphical readability.

Figure 9. *Production Quality Indicator by Weekly Production Load*

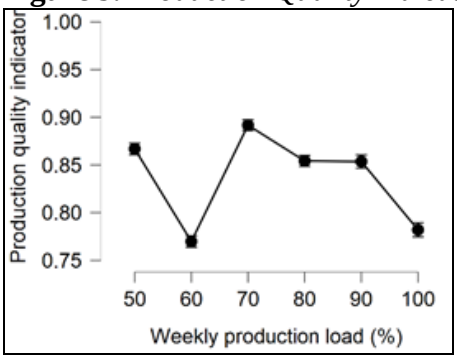

We observe that the best quality scores are achieved for a weekly production load of 70% and the lowest for 60% and 100% loads. These findings are confirmed by Tukey's pairwise comparisons which are summed up in Table 7.

Table 7. *Tukey's Post Hoc Comparisons - Weekly Production Load (%)*

Weekly Production Load (%)		Mean Difference	95% CI for Mean Difference		*t*	p_{tukey}	
			Lower	Upper			
60	50	-0.10	-0.12	-0.08	-15.20	< 0.001	***
	70	-0.12	-0.14	-0.10	-20.49	< 0.001	***
	80	-0.08	-0.10	-0.07	-14.47	< 0.001	***
	90	-0.08	-0.10	-0.07	-13.70	< 0.001	***
70	50	0.02	0.01	0.04	5.32	< 0.001	***
	80	0.04	0.03	0.05	9.69	< 0.001	***
	90	0.04	0.03	0.05	8.89	< 0.001	***
	100	0.11	0.10	0.12	21.66	< 0.001	***
100	50	-0.08	-0.10	-0.07	-15.22	< 0.001	***
	80	-0.07	-0.09	-0.06	-14.65	< 0.001	***
	90	-0.07	-0.09	-0.06	-13.60	< 0.001	***

* p < 0.05, ** p < 0.01, *** p < 0.001.
Note: Results are averaged over the levels of Daytime.
Note: The pairwise comparisons that are not presented are non-significant.

A low-quality score for a 100% production load can be understood by the fact that higher workloads lead to higher equipment utilization and therefore higher risk of breakdowns and sub-quality. On the other hand, such a low score for a 60% workload should raise questions and call for investigations to find potential sources of problem and correct them.

Effect of Daytime

Figure 10 depicts the evolution of the production quality over time; p-values and confidence intervals are adjusted for comparing a family of 12 estimates using Tukey's correction method.

Figure 10. *Production Quality Indicator over Time*

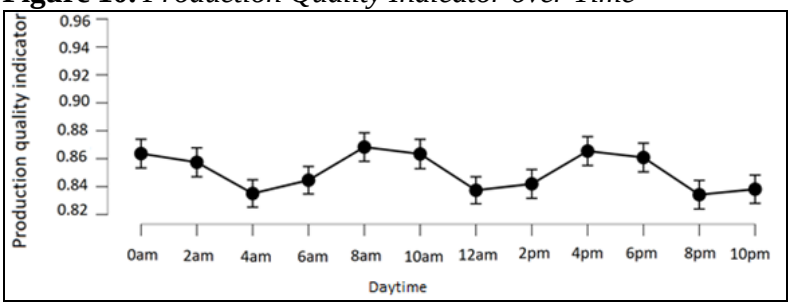

One can observe that the best quality scores are achieved for 0am, 8am, 10am, 4pm, and 6pm, and the lowest for 4am, 12am, 8pm, and 10pm. These findings are confirmed by Tukey's pairwise comparisons which are given in Table 8.

Table 8. *Tukey's Post Hoc Comparisons – Daytime*

Daytime		Mean difference	95% CI for mean difference		*t*	p_{tukey}	
			Lower	Upper			
4am	0am	-0.03	-0.05	-4.13e-3	-3.82	< 0.01	**
	8am	-0.03	-0.06	-7.79e -3	-4.32	< 0.001	***
	10am	-0.03	-0.05	-3.53e -3	-3.74	0.01	*
	4pm	-0.03	-0.05	-5.85e -3	-4.05	< 0.01	**
	6pm	-0.03	-0.05	-2.46e -3	-3.60	0.02	*
12am	0am	-0.03	-0.05	-2.10e -3	-3.55	0.02	*
	8am	-0.03	-0.05	-5.77e -3	-4.04	< 0.01	**
	10am	-0.03	-0.05	-1.51e -3	-3.47	0.03	*
	4pm	-0.03	-0.05	-3.83e -3	-3.78	< 0.01	**
	6pm	-0.02	-0.05	-4.37e -4	-3.33	0.04	*
8pm	0am	-0.03	-0.05	-5.72e -3	-4.04	< 0.01	**
	8am	-0.03	-0.06	-9.38e -3	-4.53	< 0.001	***
	10am	-0.03	-0.05	-5.13e -3	-3.96	< 0.01	**
	4pm	-0.03	-0.06	-7.44e -3	-4.27	< 0.01	**
	6pm	-0.03	-0.05	-4.05e -3	-3.81	< 0.01	**
10pm	0am	-0.02	-0.05	-2.90e -4	-3.31	0.04	*
	8am	-0.03	-0.05	-3.95e -3	-3.80	< 0.01	**
	4pm	-0.03	-0.05	-2.01e -3	-3.54	0.02	*
2pm	8am	-0.03	-0.05	-2.74e -3	-3.64	0.01	*
	4pm	-0.03	-0.05	-7.97e -4	-3.38	0.04	*

* $p < 0.05$, ** $p < 0.01$, *** $p < 0.001$

Note: Results are averaged over the levels of Weekly production load.

Note: The pairwise comparisons that are not presented are non-significant.

To conclude, the two case studies presented here illustrate some practical uses of the simulation tool in a statistics and data analysis course. We have covered some descriptive and inferential statistics topics: confidence intervals, normality tests, t-tests, homogeneity tests, Anovas. However, the diversity of the output variables (continuous, discrete, categorical) allows for more analyses (linear regression, logistic regression, multiple component analysis, and more). Another advantage of this tool is generating custom datasets to focus on a particular technique and explore its many facets.

Discussion

The simulation tool has not yet been evaluated in the Statistics and Data Analysis course. However, it was evaluated in the Advanced Management course, where it was used in hands-on work for building production indicators and improving production. Student feedback was positive regarding the industrial context of the project and the manipulation of real-world data. A qualitative analysis of the added value of the simulation tool and a rigorous quantitative analysis of the knowledge and learning gains still need to be done in both courses.

Eventually, the simulation tool will be used in several courses and at different levels of student training: in the first year for statistical analysis of data, in the second year for the optimization of manufacturing processes, and the third year for the drafting of specifications, technical and commercial communication materials, Etc.

As for future developments of the simulation tool, randomness is currently generated by uniform and Gaussian distributions, and we plan to introduce other statistical distributions for specific events (Exponential and Erlang for inter-arrival times, triangular, beta, normal, and LogNormale for service times, Weibull for inter-arrival times, Etc.) We also need to develop a user interface that will allow students to design their own data sets and quality indicators.

Conclusion

We believe that when students are actively involved in an experiment, they internalize better the material being taught and mobilize more inner resources for learning. The industrial context could help to get more commitment of the students by projecting them in their future profession and following that, to adopt a professional posture in the analysis of the problem, the choice of the data analyses to carry out, their rigorous application, and the restitution of the results in a form that is clear, concise, and adapted to the recipient.

In this vein, we proposed a simulation tool to generate realistic industrial datasets and we presented two case studies to illustrate its use in a Statistics and Data Analysis course for IE undergraduate students. The case examples focused on some common concepts in descriptive and inferential statistics. However, the

diverse nature of the output variables allows for a wider range of analysis techniques.

The simulated data can serve the analysis of the production behavior of manufacturing systems and the identification of the most significant key performance indicators (overall equipment effectiveness, capacity...). They can also be used to identify the critical phases of the production process and to understand the involvement of the physical environment in production quality.

The tool has yet to be rigorously evaluated by students, but initial positive feedback from teachers and students, allows us to consider its deployment in other courses and other levels of training.

References

Biggs J, Tang C (2011) *Teaching for quality learning at university: what the student does*, 4th Edition. McGraw Hill, New York: Open University Press.

Bryce GR (2005) Developing tomorrow's statistician. *Journal of Statistics Education* 13(1).

Carr M, Fhloinn E (2016) A project based-learning approach to teaching second-order differential equations to engineers. In *18th SEFI-MWG European Seminar on Mathematics in Engineering Education*. Brussels: SEFI.

Carrera E (2006) Engineering statistical needs an engineering curriculum: an analysis. In *ICOTS7*. Brazil.

Chottiner S (1991) Using real (intimate) data to teach applied statistics. *Statistical Association* 45: 169–169.

Cobb GW, Moore D (1997) Mathematics, statistics, and teaching. *The American Mathematical Monthly* 104(9): 801–823.

Cobb P (1999) Individual and collective mathematical development: the case of statistical data analysis. *Mathematical Thinking and Learning* 1(1): 5–43.

Davies N (2001) A new way to teach statistics to engineers. *MSOR Connections* 1(2): 7–9.

Driver R, Asoko H, Leach J, Mortimer E, Scott P (1994) Constructing scientific knowledge in the classroom. *Educational Researcher* 23(7): 5–12.

Eisner EW (1999) The uses and limits of performance assessment. *Phi Delta Kappan* 80(9): 658–660.

Elizandro D, Taha H (2007) *Simulation of industrial systems: discrete event simulation using excel/VBA*. 1st Edition. USA: Auerbach Publications.

Eskandari H, Sala-Diakanda S, Furterer S, Rabelo L, et al. (2015) Benchmarking IE programs: 2005-2015. In *2015ASEE Annual Conference and Exposition*, 14-17 June. Seattle, WA.

Farell F, Carr M (2019) The effect of using a project-based learning (PBL) approach to improve engineering students' understanding of statistics. *Teaching Mathematics and its Applications* 38(3): 135–145.

Fraser J, Teran A (2006) Benchmarking international industrial engineering programs. In *2006 ASEE Annual Conference & Exposition*, 18-21 June. Chicago, Illinois.

Fosnot CT (1996) Constructivism: a psychological theory of learning. In *Constructivism: Theory, Perspectives and Practice,* 8–33. Teachers College, Columbia University, New York.

Garfield, J, Ben-Zvi D (2007) How students learn statistics revisited: current review of research on teaching and learning statistics. *International Statistical Review* 75(3): 372–396.

Gergen KJ (1995) Social construction and the educational process. In *Constructivism*

in Education, 17–40. Erlbaum, Hillsdale, NJ.

Gratchev I, Jeng D-S (2018) Introducing a project-based assignment in a traditionally taught engineering course. *European Journal of Engineering Education* 43(5): 788–799.

Graves DH (2002) *Testing is not teaching*. Portsmouth, NH: Heinemann.

Hmelo-Silver CE (2004) Problem-based learning: what and how do students learn? *Educational Psychology Review* 16(Sep): 235–266.

Hogg RV (1991) Statistical education: improvements are badly needed. *The American Statistician* 45(4): 342–343.

Kirschner PA, Sweller J, Clark RE (2006) Why minimal guidance during instruction does not work: an analysis of the failure of constructivist, discovery, problem-based, experiential, and inquiry-based teaching. *Educational Psychologist* 41(2): 75–86.

Kuo W (2001) Educational programs for the industrial engineer. In *Maynard's Industrial Engineering Handbook, 5th edition*, 1.39–1.53. New York: McGraw-Hill.

Lang JD, Cruse S, McVey FD, McMasters J (1999) Industry Expectations of NewEngineers: A Survey to Assist Curriculum Designers. *Journal of Engineering Education* 88(1): 43–51.

Lave J, Wenger E (1991) *Situated learning: legitimate peripheral participation.* Cambridge, UK*:* Cambridge University Press.

Libman Z (2010) Integrating real-life data analysis in teaching descriptive statistics: a constructivist approach. *Journal of Statistics Education* 18(1).

Lima RM, Mesquita D, Amorim M, Jonker G, Flores MA (2012) An analysis of knowledge areas in industrial engineering and management curriculum. *International Journal of Industrial Engineering and Management* 3(2): 75–82.

Luse A, Burkman J (2018) Safely using real-world data for teaching statistics: a comparison of student performance and perceived realism between dataset types. *Journal of the Midwest Association for Information Systems (JMWAIS)* 2018(1): 2.

Neumann DL, Hood M, Neumann MM (2013) Using real-life data when teaching statistics: student perceptions of this strategy in an introductory statistics course. *Statistics Education Research Journal* 12(2): 64–75.

Nguyen AT, Nguyen NV-P (2018) Benchmarking industrial engineering programs. *Benchmarking: An International Journal* 25(4): 1194–1212.

R Core Team (2021) R: a language and environment for statistical computing. Vienna, Austria*:* R Foundation for Statistical Computing.

Ram M, Davim JP (2018) *Modeling and Simulation in Industrial Engineering*. Springer.

Russell C, Noble S, Carter J, Currier S, Wiseman R (2011) Real world, real stories: teaching quantitative methods with real life data. In *3rd International Conference on Education and New Learning Technologies (EDULEARN11)*. Barcelona, Spain, July 4-6.

Sackey SM, Bester A (2016) Industrial engineering curriculum in industry 4.0 in a South African context. *South African Journal of Industrial Engineering* 27(4): 101–114.

Scheaffer RL (2001) Statistics education: perusing the past, embracing the present, and charting the future. *Newsletter for the Section on Statistical Education* 7(1).

Schruben DL, Schruben LW (2001) *Event graph modeling with SIGMA*. 4th Edition. Custom Simulations.

Tynjala P (1999) Towards expert knowledge? A comparison between a constructivist and a traditional learning environment in the university. *International Journal of Educational Research* 31(5): 357–442.

Willett JB, Singer JD (1992) Providing a statistical "model": teaching applied statistics using real-world data. *Statistics for the Twenty-First Century* 26: 83–98.